J. Fluid Mech. (2010), *vol.* 651, *pp.* 251–294.
doi:10.1017/S0022112009993934

The effect of Reynolds number on the dynamics and wakes of freely rising and falling spheres

M. HOROWITZ† AND C. H. K. WILLIAMSON
144 Upson Hall, Cornell University, Ithaca, NY 14853, USA

(Received 14 April 2009; revised 9 December 2009; accepted 9 December 2009;
first published online 29 March 2010)

In this paper, we study the effect of the Reynolds number (Re) on the dynamics and vortex formation modes of spheres rising or falling freely through a fluid (where $Re = 100$–$15\,000$). Since the oscillation of freely falling spheres was first reported by Newton (University of California Press, 3rd edn, 1726, translated in 1999), the fundamental question of whether a sphere will vibrate, as it rises or falls, has been the subject of a number of investigations, and it is clear that the mass ratio m^* (defined as the relative density of the sphere compared to the fluid) is an important parameter to define when vibration occurs. Although all rising spheres ($m^* < 1$) were previously found to oscillate, either chaotically or in a periodic zigzag motion or even to follow helical trajectories, there is no consensus regarding precise values of the mass ratio (m^*_{crit}) separating vibrating and rectilinear regimes. There is also a large scatter in measurements of sphere drag in both the vibrating and rectilinear regimes.

In our experiments, we employ spheres with 133 combinations of m^* and Re, to provide a comprehensive study of the sphere dynamics and vortex wakes occurring over a wide range of Reynolds numbers. We find that falling spheres ($m^* > 1$) always move without vibration. However, in contrast with previous studies, we discover that a whole regime of buoyant spheres rise through a fluid without vibration. It is only when one passes below a critical value of the mass ratio, that the sphere suddenly begins to vibrate periodically and vigorously in a zigzag trajectory within a vertical plane. The critical mass is nearly constant over two ranges of Reynolds number ($m^*_{crit} \approx 0.4$ for $Re = 260$–1550 and $m^*_{crit} \approx 0.6$ for $Re > 1550$). We do not observe helical or spiral trajectories, or indeed chaotic types of trajectory, unless the experiments are conducted in disturbed background fluid. The wakes for spheres moving rectilinearly are comparable with wakes of non-vibrating spheres. We find that these wakes comprise single-sided and double-sided periodic sequences of vortex rings, which we define as the 'R' and '2R' modes. However, in the zigzag regime, we discover a new '4R' mode, in which four vortex rings are created per cycle of oscillation. We find a number of changes to occur at a Reynolds number of 1550, and we suggest the possibility of a resonance between the shear layer instability and the vortex shedding (loop) instability. From this study, ensuring minimal background disturbances, we have been able to present a new regime map of dynamics and vortex wake modes as a function of the mass ratio and Reynolds number $\{m^*, Re\}$, as well as a reasonable collapse of the drag measurements, as a function of Re, onto principally two curves, one for the vibrating regime and one for the rectilinear trajectories.

† Email address for correspondence: mh232@cornell.edu

1. Introduction and preliminary results

Whether a sphere vibrates as it rises or falls through a fluid is of interest in a number of practical applications. This phenomenon is known to affect drag as well as heat and mass transfer, which have important implications for sedimentation and other multiphase flows (e.g. Richardson & Zaki 1954; Stringham, Simons & Guy 1969; Hartman & Yates 1993), while the oscillatory motion itself can influence atmospheric measurements using weather balloons (Scoggins 1964; Murrow & Henry 1965). The earliest observation of the vibration of a rising or falling sphere was reported by Newton (1726), who studied lead and wax spheres dropped in water, as well as glass spheres and inflated hog bladders falling through air. In the case of the bladders, he observed that they 'did not always fall straight down, but sometimes flew about and oscillated to and fro while falling. And the times of falling were prolonged and increased by these motions', demonstrating that vibration causes greater drag. It was later suggested by Schmidt (1920), Hirsch (1923) and Schmiedel (1928), that these oscillatory motions are linked to periodic vortex shedding. Most subsequent studies of freely rising or falling spheres have concluded that for a given Reynolds number, the mass ratio m^* or relative density of the body compared to the fluid, determines when vibration will occur. Lighter spheres are reported to oscillate transverse to the vertical, or even to move with helical trajectories, while heavier ones move approximately rectilinearly. The sole exception to this were experiments by Karamanev, Chavarie & Mayer (1996), who suggested that the occurrence of vibration does not depend on the mass ratio, but that oscillatory motion appears when $Re/D = U/\nu > 1450\,\mathrm{cm}^{-1}$.

Preukschat (1962) concluded that falling spheres ($m^* > 1$) have a rectilinear trajectory, while rising spheres ($m^* < 1$) vibrate, over the regime $1000 < Re < 10\,000$. The oscillations would begin in a vertical plane, but would sometimes transition to a three-dimensional non-periodic motion referred to as 'spiralling'. In a recent paper, Jenny, Dušek & Bouchet (2004) performed numerical simulations over a selection of m^* from 0 to 10, and a range of Galileo number, $Ga = \sqrt{|1 - m^*|\, gD^3}/\nu$, between 150 and 350, roughly corresponding to $225 < Re < 550$. They propose that there exist at least five different regimes of sphere trajectories: oblique rectilinear trajectories, oblique trajectories which have a small oscillating component, periodic zigzag motions, chaotic trajectories and also a regime where zigzag motions or chaotic paths could both be found, depending on the initial conditions. In particular, they find the zigzag regime only below $m^* \approx 1$.

While Preukschat (1962) and Jenny *et al.* (2004) only found vibration for rising spheres, there are also a number of studies which observe that spheres can oscillate at large amplitude even when they are heavier than the surrounding fluid. For instance, Shafrir (1965) describes 'irregular corkscrew' paths, and Christiansen & Barker (1965) observe 'slightly spiral' trajectories for falling spheres. Both these descriptions appear similar to the 'spiralling' motions found by Preukschat (1962) for rising spheres. On the other hand, Kuwabara, Chiba & Kono (1983) note that spiralling motion is 'seldom observed', with falling spheres oscillating primarily in a plane. Both 'spiral' and 'zigzag' motions were found by MacCready & Jex (1964) in their experiments with spheres rising and falling through air and water. They argue that the amplitude of these oscillations ($A^* = A/D = \text{amplitude/diameter}$) should depend on both the wavelength of the body's trajectory, $\lambda^* = \lambda/D$, and the mass ratio. Employing a fit to their experimental data, they propose an approximation for the amplitude as

$$\frac{A^*}{\lambda^*/2} = \frac{0.37}{1 + 2m^*}. \tag{1.1}$$

Symbol	Study	Re	m^*
	Vibrating		
■	Preukschat (1962)	830–5400	0.53–0.95
▼	MacCready & Jex (1964)	12 000–300 000	0.03–1.52
▲	Christiansen & Barker (1965)	15 000–20 000	1.18–2.80
◆	Shafrir (1965)	1100–66 000	1.14–14.95
►	Kuwabara *et al.* (1983)	1500–41 000	1.13–7.8
●	Jenny *et al.* (2004)	230–450	0.0–0.94
	Rectilinear		
□	Preukschat (1962)	520–42 000	1.15–7.78
▽	Stringham *et al.* (1969)	15–120 000	1.14–14.95
○	Jenny *et al.* (2004)	200–310	0.0–10
△	Veldhuis & Biesheuvel (2007)	250–350	0.56–2.33
	'Chaotic'		
⊙	Jenny *et al.* (2004)	260–540	0.0–10
◬	Veldhuis & Biesheuvel (2007)	250–350	0.56–2.33

TABLE 1. Reynolds numbers and mass ratios studied in previous investigations of rising and falling spheres. Types of motion reported are mapped in the mass ratio – Reynolds number plane in figure 2. Vibrating cases shown with solid symbols; rectilinear motion shown with open symbols; random, 'chaotic' motions shown with bullseye symbols. Reynolds numbers were not provided by Jenny *et al.* (2004) and Veldhuis & Biesheuvel (2007), and were estimated from reported values of Ga.

A typical wavelength for zigzagging motion is cited as of the order of $\lambda^* = 12$. Therefore, according to (1.1), amplitudes for falling spheres as large as $A^* = 0.7$ are predicted. The Reynolds numbers for these studies are typically of the order $Re \sim 1000$–$10\,000$, as shown in table 1. At lower Reynolds numbers, several images from the Schlieren visualization study of Veldhuis *et al.* (2005) suggest that falling spheres also vibrate. However, in subsequent experiments in which trajectories are measured (Veldhuis & Biesheuvel 2007), they find that zigzagging motion does not occur consistently. Instead, for rising spheres, vibration occurs for some experimental runs, while others exhibit random motion similar to the 'chaotic' regime of Jenny *et al.* (2004). For falling spheres, only chaotic motion was observed.

The types of motion found in these previous studies are summarized in figure 1, for those investigations where $\{m^*, Re\}$ data is available. In some cases, the Reynolds number was estimated from reported values of the Galileo number (the use of Galileo number instead of the Reynolds number is discussed in the Appendix). The types of motion observed may be distinguished from the symbols: solid symbols refer to large-amplitude vibration, open symbols correspond to motion that is essentially rectilinear and bullseye symbols are used to denote random transverse ('chaotic') motions. One important feature of this map is that *vibration or 'chaotic' motion is found for all rising spheres* ($m^* < 1$). This statement is applicable for Re above the threshold where vortex shedding is found, which for a fixed sphere, occurs at $Re > 275$. It is also worth noting that most of the previous investigations shown here are restricted to a relatively narrow range of mass ratio or Reynolds number. None have attempted to provide a comprehensive description of the changes that occur over the range of Re spanned in this map. Moreover, there has been very little work on light spheres ($m^* < 0.6$), especially at Reynolds numbers greater than $Re \approx 500$. It is evident in figure 1 that even for Reynolds numbers where there has been some study

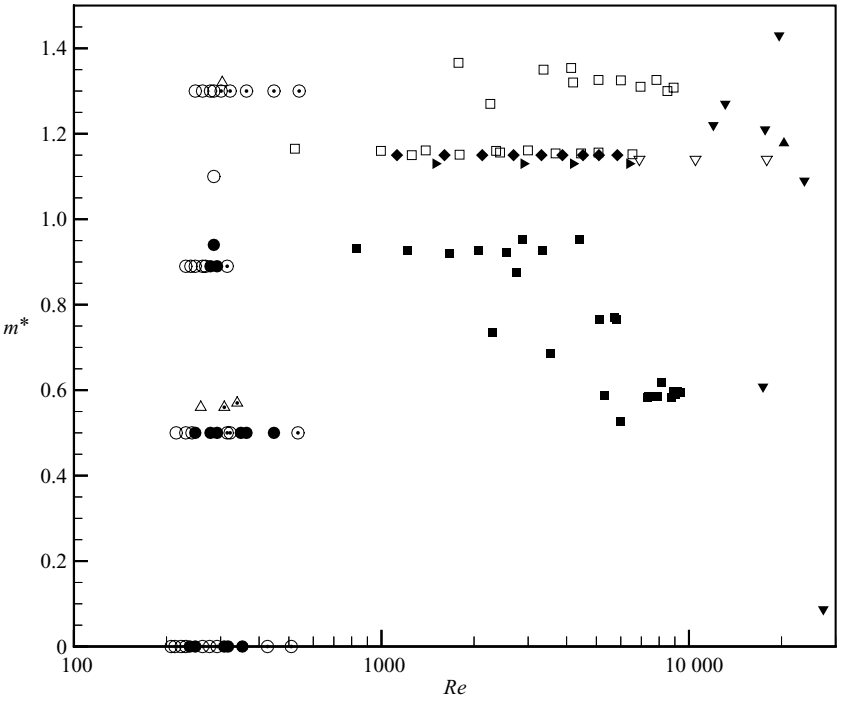

FIGURE 1. Regimes of motion found in previous studies of freely rising and falling spheres, mapped in the $\{m^*, Re\}$ plane. Symbols correspond to studies in table 1: solid symbols indicate vibration, open symbols indicate rectilinear motion, and bullseye symbols indicate 'chaotic' motion.

Symbol	Study	Re	m^*
◀	Karamanev *et al.* (1996)	180–20 000	0.03–0.92
⋆	Allen (1900)	2300–8300	7.66–7.81
▷	Liebster (1927)	0.13–2400	6.03–9.14
+	Lunnon (1928)	1600–150 000	7.69–10.5
×	Boillat & Graf (1981)	140–13 000	1.02–2.70
◁	Veldhuis, Biesheuvel & Lohse (2009)	150–2050	0.02–2.63

TABLE 2. Additional studies reporting drag coefficients of rising and falling spheres. Drag data for these experiments, as well as for many of the studies listed in table 1, are plotted in figure 2.

of light bodies, the resolution in mass ratio is quite coarse. Due to the sparseness of the mass ratio data, we cannot draw conclusions about where transitions in the dynamics occur.

Our map of sphere dynamics based on previous results also demonstrates that there is substantial disagreement between different studies. For example, Shafrir (1965) and Kuwabara *et al.* (1983) stated that a sphere at $m^* = 1.15$ and $Re = 6000$ would vibrate. On the other hand, Preukschat (1962) and Stringham *et al.* (1969) found that a sphere with these parameters moves rectilinearly. This disagreement also extends to quantities such as the drag coefficient, which are affected by vibration. In figure 2, we plot drag measurements for the studies in tables 1 and 2, performed under laboratory conditions. Here we exclude some early results from spheres dropped in uncontrolled environments (Shakespear 1914; Bacon & Reid 1923; Lunnon 1926).

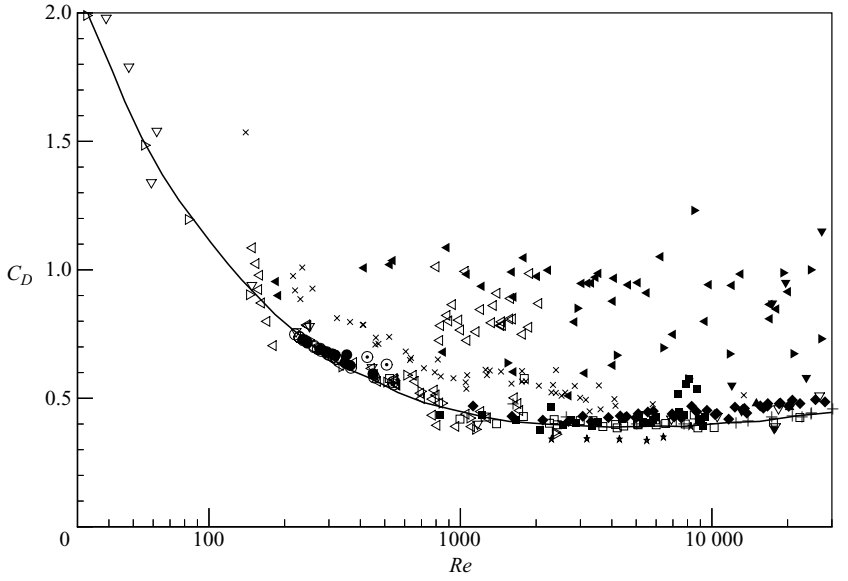

FIGURE 2. Mean drag coefficients from previous studies of freely rising and falling spheres. Symbols as in tables 1 and 2; —, drag of stationary sphere compiled the book by Schlichting (1955), where he plots original data from Wieselsberger (1921) and Liebster (1927).

However, despite the possibility of some control over experimental conditions in the studies of figure 2, there is substantial scatter in this data. Some spheres said to be vibrating have drag coefficients quite close to the drag on a stationary body (e.g. Shafrir 1965), while in other cases, large drag increases are reported for oscillatory motion (MacCready & Jex 1964; Karamanev *et al.* 1996), consistent with the original observations by Newton (1726).

Such significant differences between previous results suggest that a key question remains: *Under what conditions does a rising or falling sphere vibrate?* In order to address this question, we will also need to determine what types of motion exist. Even when spheres are found to vibrate, some studies have found motion in a single plane, while others describe three-dimensional 'spiralling' trajectories. In some cases random 'chaotic' paths are found. A key part of the present work will be precise identification of the regimes of motion for different mass ratios and Reynolds numbers.

We begin our study with a set of preliminary experiments at $Re \approx 10\,000$ (based on the terminal velocity), performed in the facility described in § 2. In figure 3, we show views of the sphere trajectories from the front and from the side of the tank, as well as Lissajous figures where only the fluctuating part of the motion is plotted. In our coordinate system, gravity always points in the vertical $-X$ direction. The Y and Z axes are horizontal, and chosen such that the transverse motion of the sphere lies principally in the Y direction. In all cases, the sphere was released four diameters before the start of the recorded trajectories shown here. A falling sphere, with $m^* = 2.84$, descended essentially vertically, with very small non-periodic fluctuations. For a buoyant sphere with $m^* = 0.75$, one would predict, based on the map in figure 1, that vibration would occur. Instead, after undergoing a brief initial transient, the sphere rose rectilinearly. This intriguing result demonstrates that contrary to previous studies, rectilinear trajectories can occur for rising spheres, just as they do for falling ones. Only when the mass ratio was reduced further, did the

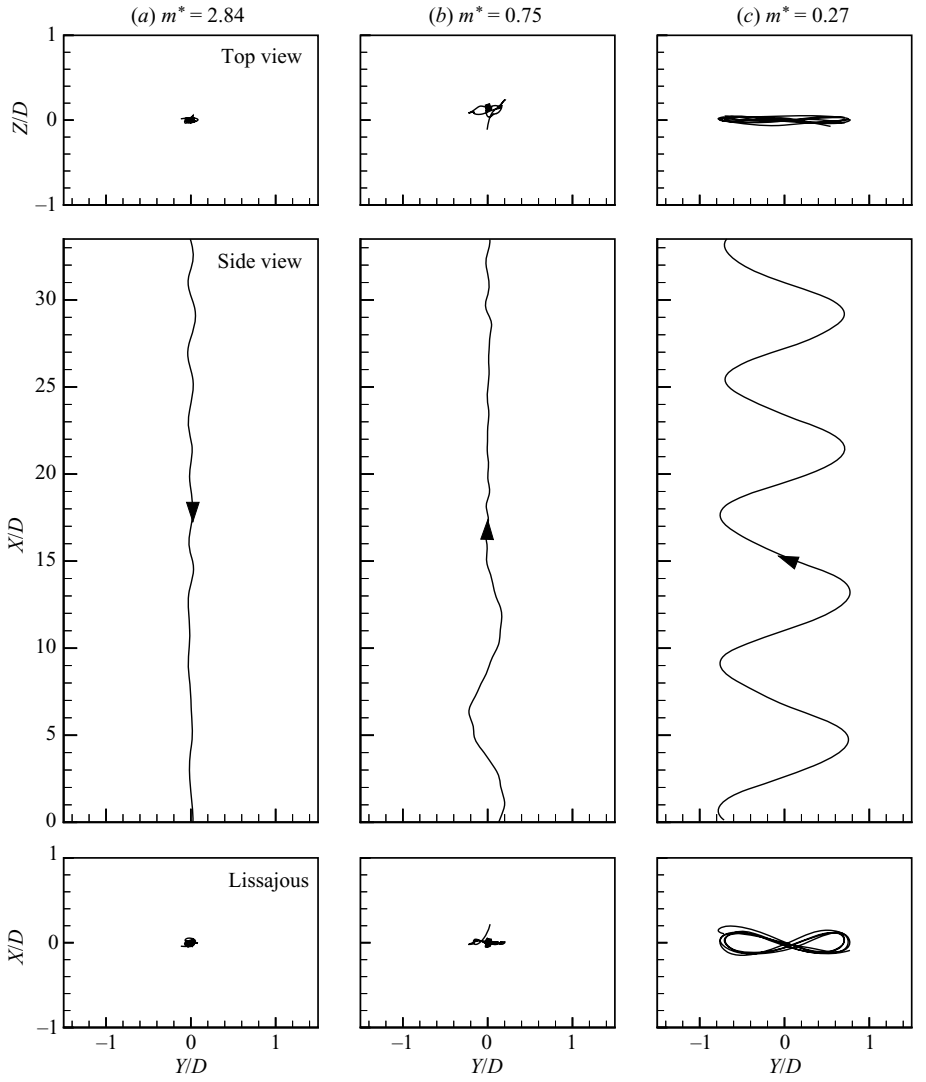

FIGURE 3. Lissajous and trajectories in the X–Y (side view) and Y–Z (top view) planes for spheres at $Re \approx 10\,000$. (a) $m^* = 2.84$; falling spheres descend vertically. (b) $m^* = 0.75$; a rising sphere ascends with a rectilinear trajectory, following a short transient. (c) $m^* = 0.27$; a very light rising sphere undergoes large-amplitude periodic vibrations in a single plane. The end of the release mechanism is located four diameters from the start of the trajectories shown here. In all cases, it should be noted that the Y-axis of the trajectory is significantly expanded relative to the X-axis, so that the actual transient motions in (a) and (b) are very small.

sphere suddenly began to vibrate vigorously. We show this distinct periodic zigzag vibration for a sphere with $m^* = 0.27$ in figure 3(c). Such large-amplitude highly periodic oscillations always occurred in a vertical plane, independently of how the sphere was released.

The initial results from these experiments suggest that the regime of periodic vibration occurs over a narrower range of mass ratio than previously thought. This is further explored in § 3, where we employ spheres with many different mass ratios to obtain a precise value for the transition between regimes. From amplitude

measurements of these spheres, (all at $Re \approx 10\,000$, as in our example in figure 3) we find a critical mass ratio separating rectilinear motion from periodic vibration at $m^*_{crit} = 0.61$. We also relate the phenomenon of spheres oscillating as they rise to the problem of vortex-induced vibration. Our previous studies (Govardhan & Williamson 2000, 2005) triggered our interest in the dynamics of freely rising and falling bodies, such as cylinders (Horowitz & Williamson 2006, submitted), or the present case of spheres. Initially, in this paper, we consider the effect of Reynolds number using experiments at $Re = 450$. Here we find a distinctly lower critical mass, $m^*_{crit} = 0.36$, than we did at $Re = 10\,000$, where its value was 0.61. The dependence of the dynamics on Reynolds number shown by these two cases is explored further, over the range $Re = 100$–$15\,000$, where we map the regimes of motion that occur in the $\{m^*, Re\}$ plane in § 3.

Since the wake and body motion of a rising sphere will interact, one expects that vibration will result in a different vortex wake mode than for the same body moving rectilinearly, or held stationary in a free stream. Therefore, one may ask: *What modes of vortex formation exist for a vibrating freely rising or falling sphere?*

Visualizations by Schmiedel (1928) and Schlieren images by Veldhuis *et al.* (2005) and Veldhuis & Biesheuvel (2007) indicate the formation of vortex loops and streamwise vortex filaments in the wake of freely rising and falling spheres, but specific wake modes comprising these structures have not been defined, or linked to particular types of motion. However, patterns of similar vortex structures have been observed in other similar flows. For example, single-sided chains of vortex loops are well documented in the wakes of fixed spheres in experiments (Möller 1938; Sakamoto & Haniu 1990; Leweke *et al.* 1999; Brücker 2001; Gumowski *et al.* 2008) and in computations (Johnson & Patel 1999; Mittal 1999; Tomboulides & Orszag 2000; Fabre, Auguste & Magnaudet 2008). Tethered or elastically mounted spheres (Govardhan & Williamson 2005) and liquid drops (Magarvey & Bishop 1961*a*,*b*) have also been found to shed double-sided chains of vortex loops or rings. In the case of spherical or ellipsoidal rising bubbles, for which both helical and zigzag oscillations have been observed, the principal structure of the wake when the body vibrates is shown to be pairs of counter-rotating streamwise vortices (Brücker 1999; Mougin & Magnaudet 2002). (We also note that Jenny *et al.* (2004) compute the flow field around freely moving spheres, where they present surfaces of the streamwise velocity. In the present context, it is not clear how to deduce vorticity formation modes from such velocity surfaces, though it is readily observed that periodic modes are found in their computations.) Thus, there still exist distinct differences, among the different studies, regarding the wake modes found for freely moving spheres. Further detailed visualizations and vorticity measurements would be useful to precisely identify these patterns.

Some initial results of our flow visualizations, which provided motivation for a more comprehensive study of rising and falling sphere wakes, are shown in figure 4. These experiments were performed at Reynolds number, $Re = 450$, where the wake is laminar and where visualizations are more readily achieved. The wake of a sphere falling without vibration (figure 4*a*) appears to comprise a single-sided chain of vortex loops, resembling the wake of a fixed sphere at comparable Reynolds numbers. A very light rising sphere, however, exhibits a new mode of vortex formation (figure 4*b*). In this mode, four distinct vortex structures are generated in each cycle of oscillation, twice as many structures per cycle of motion as have been observed in the wakes of fixed or tethered bodies. A preliminary investigation of this wake in (Horowitz & Williamson 2008) provided evidence that these structures are vortex rings. In § 4, we will provide a more detailed description of the structure and origin of this four-ring

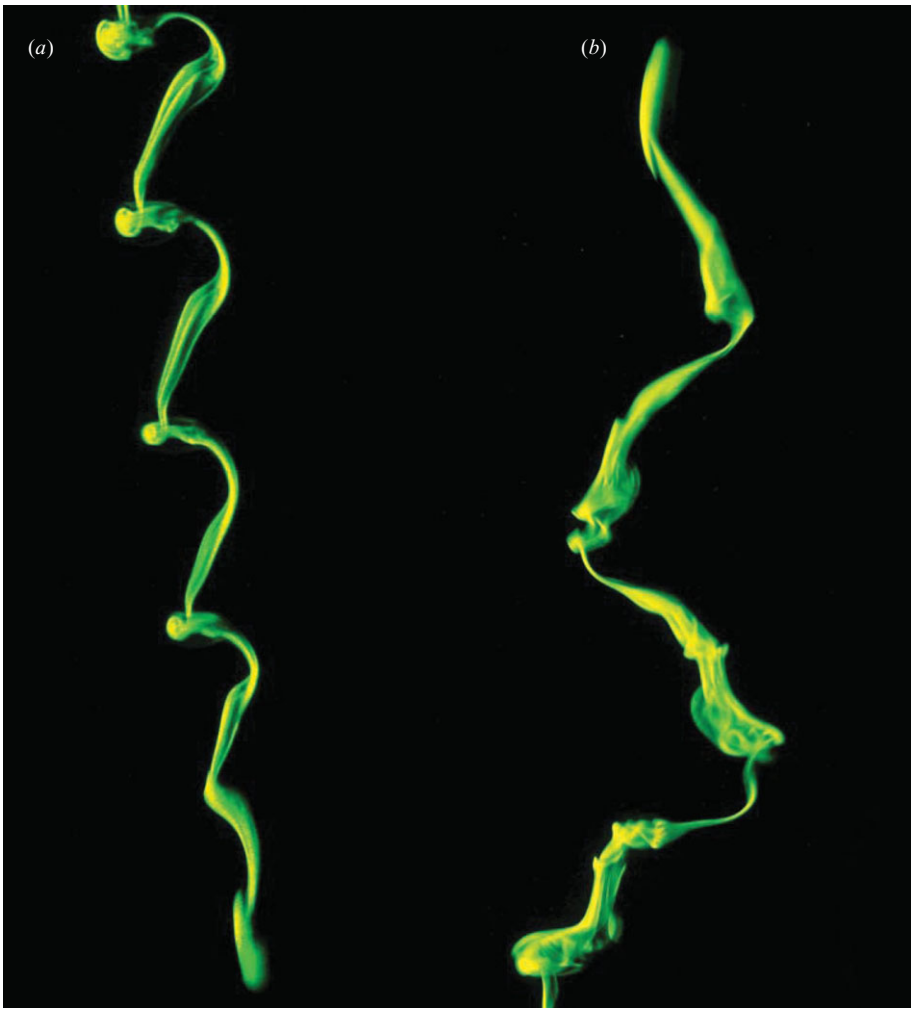

FIGURE 4. Preliminary visualizations of wakes of rising and falling spheres at $Re = 450$. (*a*) A falling sphere sheds a single-sided chain of vortex loops. (*b*) A new mode of vortex formation for a vibrating sphere, rising through a fluid, with four distinct vortex structures created in each cycle of oscillation.

'4R' mode, and present the vortex patterns found for the other regimes of motion. These periodic wake modes are classified based on the number of vortex rings produced per wavelength.

In § 5, we examine the effect of background disturbances on the sphere trajectories and on the observed regimes of motion. After the conclusions are presented in § 6, we present the appendices, comprising additional measurements of the amplitude, wavelength and phase of vibration, in particular to highlight an apparent boundary marking a change in the wake characteristics at $Re = 1550$. This is followed by a short discussion of the use of the Galileo number to map the different types of motion.

2. Experimental details

Our experiments using freely rising and falling spheres were performed in two vertical tanks with transparent walls. The larger of the two tanks had dimensions

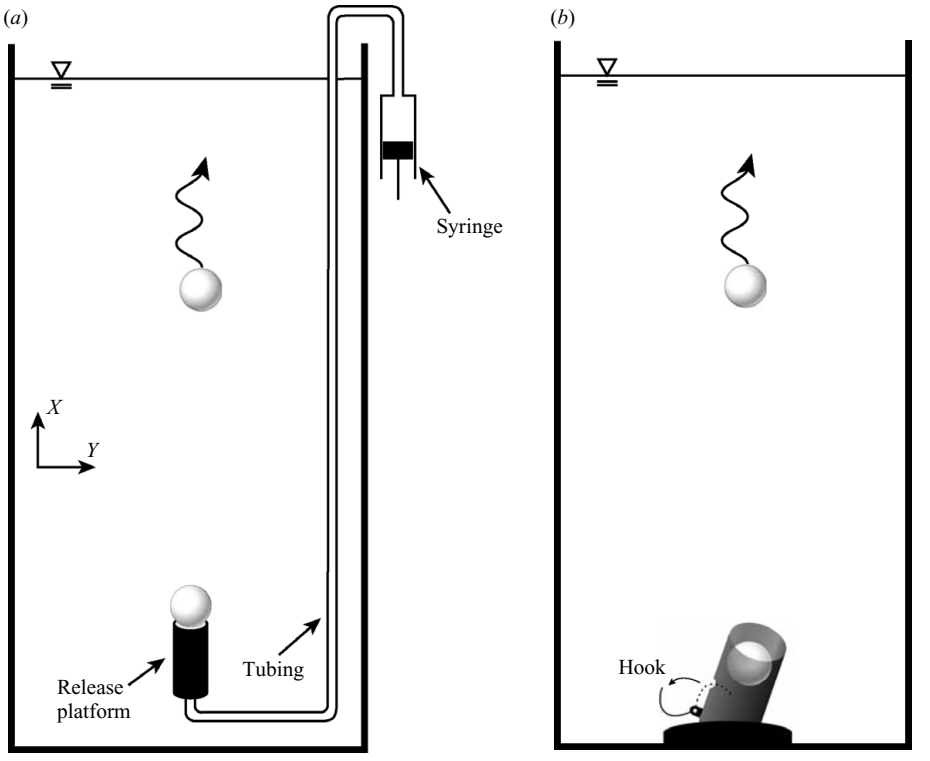

FIGURE 5. Schematic of the vertical tank and release mechanisms for a rising sphere. (*a*) The sphere rests on a cylindrical platform connected to a syringe, which applies just enough suction to keep it at the bottom of the tank. (*b*) The sphere is restrained inside a tube using a rubber-tipped hook.

0.4 m × 0.4 m × 1.5 m, while the smaller tank measured 0.2 m × 0.2 m × 0.9 m. Both solid and hollow spheres were used, and were constructed from aluminum and a variety of plastics, including nylon, polypropylene, polystyrene, acetal and phenolic. Their diameters D were between 0.2 and 3.8 cm. All of these bodies were highly spherical. The largest deviated from perfect sphericity by no more than 1.0 %, while the smallest deviated by no more than 1.5 %, as determined from multiple images of each sphere viewed from different directions, using a camera with the lens mounted on a long extension tube for high magnification. The Reynolds number was varied using mixtures of glycerin and water to control the viscosity, ν. The viscosity was measured with a Brookfield viscometer and monitored daily to account for temperature changes. These measurements were compared to tabulated viscosity data, compiled by the glycerin manufacturer for various temperatures and mixture fractions, and were determined to be different by less than 5 %.

Buoyant rising spheres were gently restrained at the bottom of the tank and were released from rest after the fluid had settled, typically two hours after previous experimental runs (we shall later see that such time delay between experiments is key to all our results presented in this paper). Two release mechanisms were used, as shown schematically in figure 5. In the first mechanism, a syringe would apply a small amount of suction to a tube on top of which the sphere would rest. The other held the sphere mechanically inside a tube using a thin rubber-tipped hook. When the hook was released, the sphere would rise out of the tube. Both mechanisms could also be inverted and placed at the top of the tank for experiments using falling spheres.

Video from two synchronized cameras placed at the front and side of the tank allowed trajectories to be determined in three dimensions as a function of time. From these trajectories, the amplitude, frequency, wavelength and terminal velocity of the sphere were calculated. Frequencies of vibration were determined from the trajectory data, and may be put as a normalized frequency parameter, $F = fD/U$. This frequency F is inversely proportional to the normalized wavelength $\lambda^* = U/fD$, which is presented throughout the paper, and plotted specifically in Appendix A, for example. The terminal velocity U was typically reached by a distance $X/D \sim 8$ after being launched, except for spheres exhibiting an initial transient motion, such as the case shown in figure 3(b), where one may only reasonably define a mean rise or fall velocity after the decay of the transient. All Reynolds numbers were calculated based on the terminal velocity U, $Re = UD/\nu$, where ν is the kinematic viscosity.

Flow visualizations for freely rising spheres were performed using a small cylinder containing sodium fluorescein dye, placed at the bottom of the tank, through which the sphere would rise after its release. Dye would be entrained in the wake of the sphere, and then illuminated with a 5 W continuous argon ion laser. Additional visualizations involved spheres undergoing a prescribed motion in a computer-controlled XY towing tank. In these experiments, dye was painted onto the sphere prior to the experiment, after which the sphere was slowly lowered into the tank. The towed sphere had a diameter of 3.8 cm and was supported by a thin rigid rod with a diameter of 0.13 cm.

The sphere wakes were studied further in the towing tank using particle image velocimetry (PIV). The fluid was seeded with 14 μm silvered glass spheres and illuminated by a sheet of laser light. Images were acquired with a JAI CV-M2CL video camera (1600 × 1200 pixels) at 30 frames s^{-1}. Image pairs were correlated with a two-step windowing process incorporating window shifting to determine particle displacements, and in turn, velocity fields. For the first correlation, interrogation windows of 64 × 64 pixels were used, with 32 × 32 pixel windows for the second correlation. Typical velocity fields comprised 80 × 60 velocity vectors, using a window overlap of 38 % in the second correlation. Further details pertaining to the particle seeding density and to the implementation of the cross-correlation technique may be found in Govardhan & Williamson (2000). Vorticity fields from individual runs are presented in this paper for laminar flow Reynolds numbers, as well as for turbulent flow ($Re = 6000$). In these cases, vorticity fields were phase averaged over approximately 10 experimental runs to remove small-scale turbulent fluctuations, while preserving the large-scale periodic structures.

3. Critical mass and regimes of motion

The preliminary experiments presented in § 1 showed that, contrary to earlier studies, there exist some rising spheres that ascend in a rectilinear path, without vibration or apparent chaotic motions. In this section, we determine the critical value of the mass ratio, m^*_{crit}, at which trajectories switch from rectilinear motion to vigorous periodic vibration as the mass is reduced, first at $Re \approx 10\,000$, and then at $Re = 450$. We then consider the effect of Reynolds number on the sphere motion, in the range of $Re \approx 100$–$15\,000$, and identify boundaries between the different regimes of motion that exist in the parameter space of m^* and Re.

3.1. *Critical mass at* $Re \approx 10\,000$

From the trajectories presented in figure 3, it is clear that a rising sphere undergoes a transition from a vertical rectilinear trajectory to periodic vibration at some mass

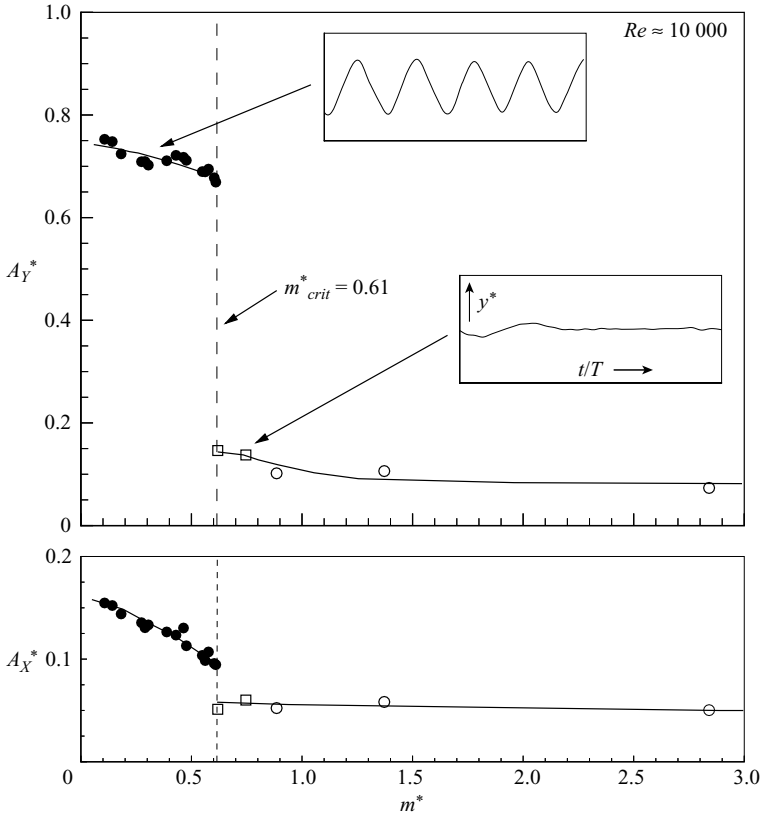

FIGURE 6. Critical mass for a sphere at $Re \approx 10\,000$. Above a critical value of the mass ratio, $m^*_{crit} = 0.61$, all falling spheres and a wide range of rising spheres move rectilinearly. Below the critical mass, the sphere vibrates vigorously. Time histories of the transverse displacement, $y^* = y/D$, are shown inset for selected mass ratios.

ratio between 0.27 and 0.75, at a Reynolds number of 10 000. By systematically varying m^* and measuring the amplitude of the horizontal (transverse) motion A^*_Y, we can determine the critical mass at which this transition between regimes occurs. Based on the amplitude measurements presented in figure 6, we evaluate a critical mass

$$m^*_{crit} = 0.61 \pm 0.02, \tag{3.1}$$

for $Re \sim 10\,000$. All spheres heavier than this critical mass move rectilinearly (with a small amount of intermittent transverse motion when close to the critical mass). Upon reducing the mass below m^*_{crit}, the sphere suddenly begins to oscillate with a peak-to-peak amplitude around one and a half diameters ($A^*_Y \approx 0.75$). In all of the experiments where the sphere vibrated, the motion was confined to a single vertical plane, even though the sphere was free to move in three dimensions. Three-dimensional or 'spiralling' trajectories have sometimes been reported for rising spheres (e.g. by Preukschat 1962), but the planar oscillations we observed were highly robust, occurring for every experimental run, and with a consistent amplitude and wavelength.

In addition to the transverse oscillations evident from the trajectory of the vibrating sphere in figure 3(*c*), the Lissajous figure shows that there also exists periodic streamwise vibration, defined by an amplitude A^*_X, and at a frequency twice that

of the transverse direction. Such streamwise motions have been reported for rising cylinders (Horowitz & Williamson 2006, submitted), flat cylinders (Fernandes *et al.* 2007) and spheroidal bubbles (Mougin & Magnaudet 2006). Although this appears to be the first time they have been observed for a spherical body, streamwise oscillations should indeed be expected. These streamwise fluctuations are not immediately evident from the trajectories, because they are considerably smaller than the mean vertical velocity. Only in the Lissajous figure, in which the effect of the mean velocity is removed, leaving solely the fluctuating part of the motion, do they become apparent. This streamwise vibration is always found for spheres oscillating in the transverse direction, appearing suddenly at m^*_{crit}.

The existence of a critical mass ratio, at which different regimes of motion are separated by an abrupt jump, is not unique to rising and falling bodies. Such a phenomenon has also been found in the case of elastically mounted and tethered bodies undergoing vortex-induced vibration (VIV) transverse to a free stream (Govardhan & Williamson 2000, 2002, 2005; Williamson & Govardhan 2004). It turns out that an unrestrained freely rising body represents a special case of an elastically mounted VIV system, one in which there is no stiffness or damping (Horowitz & Williamson 2006, submitted).

To relate a rising sphere to elastically mounted VIV systems, we must first consider its equation of motion,

$$m\ddot{y} = F_Y(t). \tag{3.2}$$

Since the body vibration is synchronized with the periodic wake formation, the displacement and force may be approximated as sinusoidal, with a frequency f. If we normalize (3.2), we obtain

$$m^* = -C_{EA}. \tag{3.3}$$

The quantity C_{EA} is a non-dimensional apparent added mass, proportional to the force in phase with the body acceleration according to

$$C_{EA} = -\frac{3}{16\pi^2}\frac{C_Y}{A^*_Y}\lambda^{*2}. \tag{3.4}$$

It includes contributions from the fluid force due to the dynamics of vorticity, as well as an (ideal) added mass force arising from acceleration of the fluid around the body. All vibrating spheres must satisfy (3.3). Therefore, vibration can only exist for mass ratios below some maximum negative value of C_{EA}. In other words, the critical mass is given by

$$m^*_{crit} = [-C_{EA}]_{max}. \tag{3.5}$$

The value of the apparent added mass C_{EA} is dependent on the vortex dynamics. Recalling that a rising sphere is a particular case of an elastically mounted sphere undergoing VIV, it is possible evaluate $[-C_{EA}]_{max}$ from measurements of such a VIV system. For an elastically mounted body, the apparent added mass is defined as

$$C_{EA} = \frac{3}{16\pi^2}\frac{C_Y\cos\phi}{A^*_Y}\lambda^{*2}, \tag{3.6}$$

where ϕ is the phase between the force and displacement (note that if $\phi = 180^\circ$, i.e. if the force is in phase with acceleration, we obtain (3.4)). Generalized equations, such as (3.6) can be found in Govardhan & Williamson (2005). Also in that paper, values of C_{EA} from elastically mounted sphere experiments were calculated, and are presented in figure 7. These measurements indicate that $[-C_{EA}]_{max}$ is between -0.55 and -0.65.

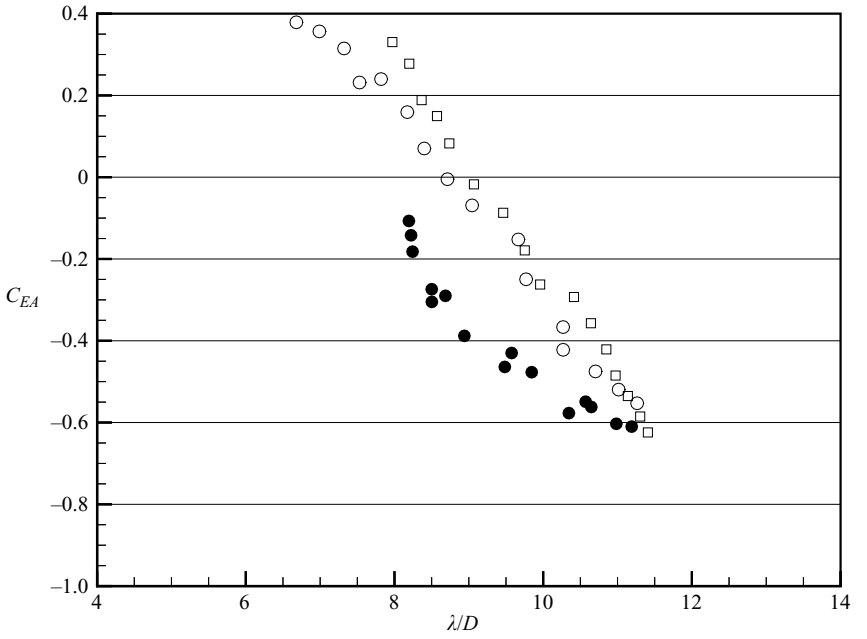

FIGURE 7. Using the apparent added mass, C_{EA} to evaluate the critical mass. Tethered and elastically mounted spheres (Govardhan & Williamson 2005) have a maximum negative value of $-C_{EA} \approx 0.6$, in good agreement with the critical mass of a rising sphere, $m^*_{crit} = 0.61$. ●, freely rising sphere, $Re \approx 8000$–$14\,000$; ○, tethered sphere, $m^* = 2.83$, $Re \approx 3200$–7800; □, elastically mounted sphere, $m^* = 1.31$, $Re \approx 10\,000$–$23\,000$.

Therefore, from measured values of C_{EA}, we predict a critical mass, $m^*_{crit} = 0.6 \pm 0.05$. This value is in remarkably good agreement with the critical mass obtained for freely rising spheres at comparable Reynolds numbers, $m^*_{crit} = 0.61 \pm 0.02$, in this study.

3.2. *Critical mass and dynamics at* $Re = 450$

In this section, we begin our investigation into the effect of Reynolds number on the dynamics of rising and falling spheres by studying the problem at $Re = 450$. Based on observations of fixed spheres, the wake at this Reynolds number should be laminar, and one might expect the dynamics to differ from the previous case of $Re = 10\,000$, for which the wake is turbulent. In essence, the value of C_{EA}, and therefore critical mass, is dependent on the vortex-induced forces, which are a function of Reynolds number, so one expects some differences in critical mass for lower Re.

Amplitude measurements at $Re = 450$ indicate a critical mass $m^*_{crit} = 0.36 \pm 0.03$, as shown in figure 8. This value is distinctly lower than the one at $Re = 10\,000$, where we find $m^*_{crit} = 0.61$, which confirms that the dynamics are dependent on Reynolds number. One of the interesting results of the experiments at higher Re was the discovery of rectilinear trajectories for rising spheres. With a smaller critical mass at $Re = 450$, rising spheres will move rectilinearly over a greater regime of relative densities.

Trajectories for the types of motion found at $Re = 450$, are shown in figure 9. Unlike the higher Reynolds number case, spheres moving rectilinearly do not have trajectories that are vertical. Instead, the trajectories are oblique, indicating that a lift force with a non-zero mean is acting on the body. In the case of the lighter vibrating spheres, the periodic zigzag motion resembles the dynamics at higher Re,

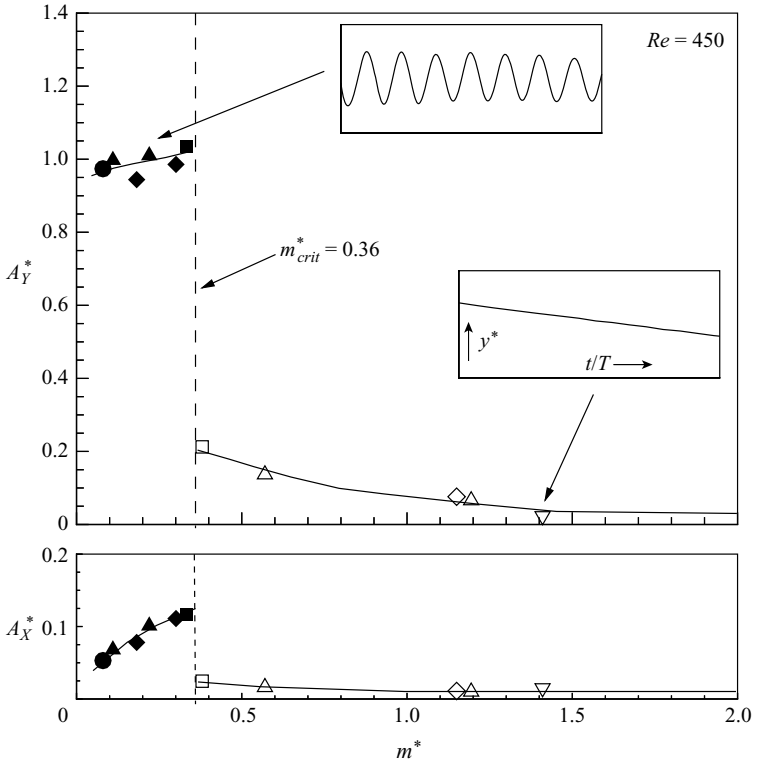

FIGURE 8. The critical mass at $Re = 450$ occurs at $m^*_{crit} = 0.36$. This value is distinctly lower than at $Re \approx 10\,000$ (where $m^*_{crit} = 0.61$), indicating a clear dependence of the critical mass on the Reynolds number. Periodic vibration: ●, $D = 0.3$ cm; ■, $D = 1$ cm; ▲, $D = 1.3$ cm; ◆, $D = 2$ cm. Oblique, rectilinear motion: ▽, $D = 0.5$ cm ; □, $D = 1$ cm; △, $D = 1.3$ cm; ◇, $D = 2$ cm.

always being confined to a single plane. Although it is well known that bubbles rising through a liquid at comparable Reynolds numbers may move with helical trajectories (see e.g. the review of Magnaudet & Eames 2000), we found no evidence of spiralling motion in any experiment we conducted.

These results were found to be independent of the initial conditions. By adjusting the inclination angle of our release platform, we could impart a small initial horizontal velocity on the sphere. The trajectories shown in figures 9(*e*) and 9(*f*) are for the release mechanism angled at 0° (vertical) and at 20°. Both cases exhibit the same resulting zigzag motion. The only apparent effect of the initial conditions was to determine the orientation of the vertical plane in which the light spheres vibrated. Nor was the motion influenced by the sphere diameter relative to the tank dimensions. Experiments using spheres with different diameters, but similar mass ratios, as shown for example in figures 9(*d*) and 9(*e–f*), yield closely similar dynamics. This consistency between different body diameters is also illustrated by figure 8, where different symbols are used for each sphere size. While sphericity varied slightly for these experiments, within the fine tolerances of the spheres used (between 1 and 1.5 % deviation from perfect sphericity), there was no apparent effect on the motion.

Despite our imposed variation of the initial conditions and body diameter, the vibration of the light spheres was extremely periodic. To demonstrate the clear periodicity, we plot in figure 10 the measured time histories of the transverse

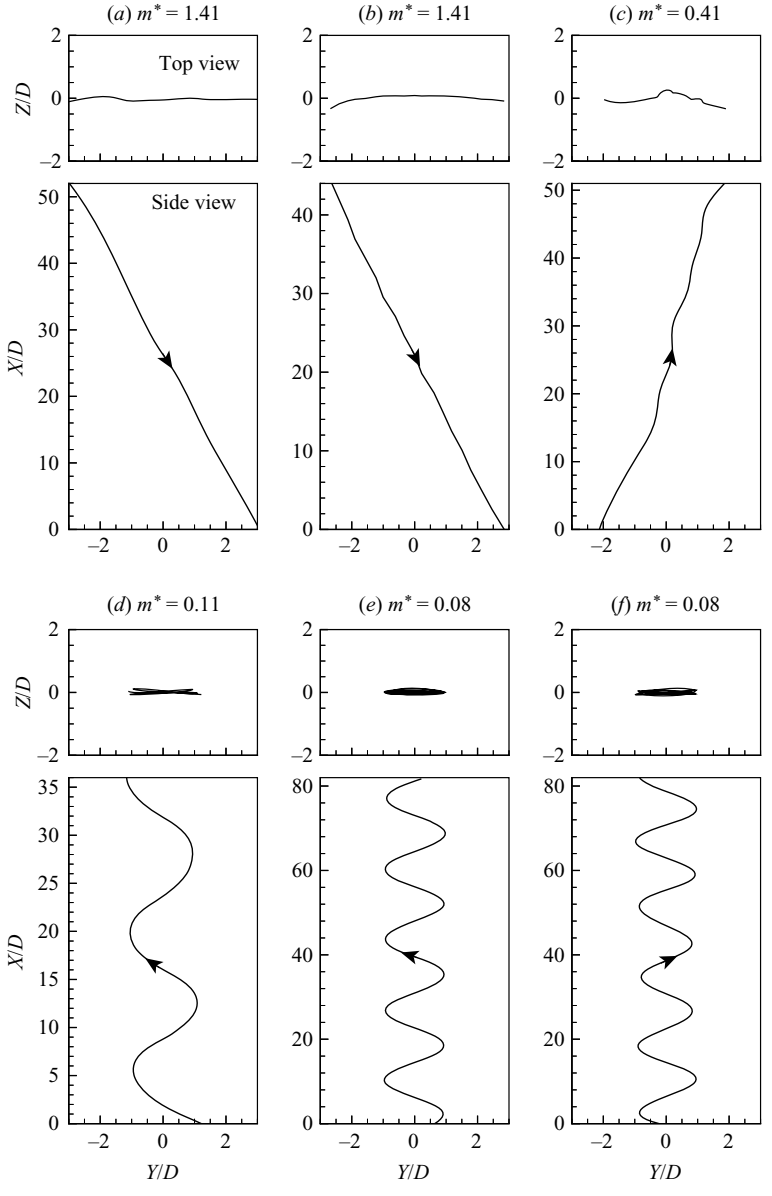

FIGURE 9. Trajectories of rising and falling spheres at $Re = 450$. (*a–b*) $m^* = 1.41$; falling spheres always descend in an oblique, rectilinear path. The two runs shown here demonstrate the repeatability of this motion. (*c*) $m^* = 0.41$; a rising sphere with an oblique trajectory. (*d*) $m^* = 0.11$, $D = 1.3$ cm. (*e*) $m^* = 0.08$, $D = 0.3$ cm, release mechanism inclined at 0° from vertical; (*f*) $m^* = 0.08$, $D = 0.3$ cm, release mechanism inclined at 20° from vertical. In (*d*)–(*f*), we see highly periodic zigzag trajectories through the fluid, which are contained in a vertical plane.

displacement, on top of which we have superposed an average precisely periodic motion. The average motion was calculated by splitting the measured trajectory into individual cycles (four to five cycles in the cases presented here in figure 10) and taking their mean. At both Reynolds numbers shown in figure 10, the measured

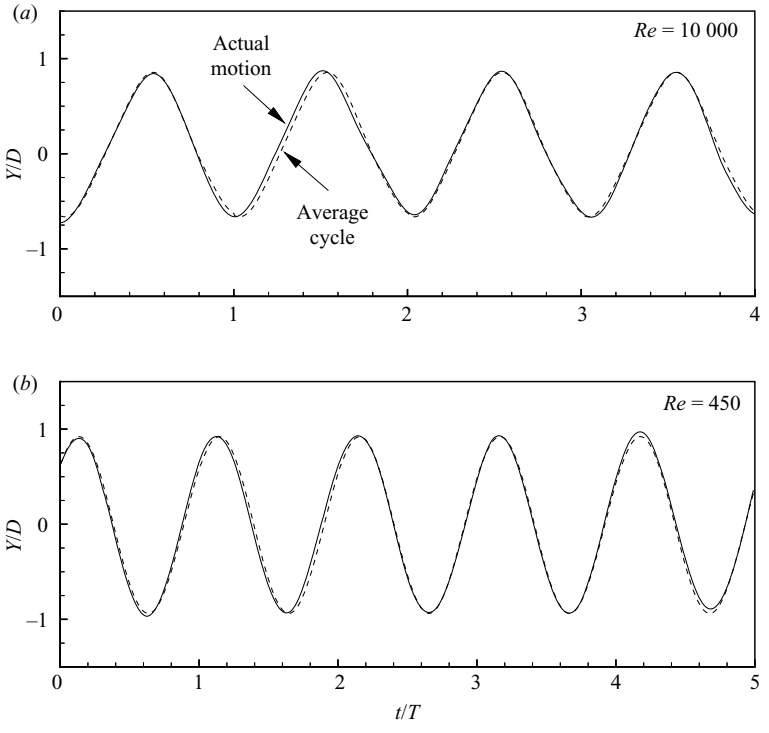

FIGURE 10. Time histories of transverse vibration compared to the average cycle of motion. These time histories demonstrate the high periodicity of the zigzag regime, as the sphere shows no sign of departing from the average motion over time. (*a*) $Re = 10\,000$. (*b*) $Re = 450$.

transverse displacement always lies very close to the average cycle. The amplitude remains essentially constant throughout the duration of the experiment; cycle-to-cycle differences in the frequency are minimal. The motion shows no sign of drifting from this average cycle, let alone undergoing an abrupt change in dynamics (which has been reported in previous studies), and appears to be indicative of steady-state behaviour.

3.3. *Regimes of motion in the* $\{m^*, Re\}$ *plane*

In our experiments on freely rising spheres at $Re = 450$ and 10 000, we find that the Reynolds number has an impact both on the critical mass and on the types of motion that occur. This effect, however, could not possibly be interpreted from the map of previous studies shown in figure 1. In an effort to clarify the dynamics of spheres in the $\{m^*, Re\}$ plane, we have investigated 133 different combinations of mass ratio and Reynolds number. The results of this study, presented in figure 11, are the product of nearly 690 individual experimental runs. These experiments took a substantial period of time to complete, if one considers the need to wait hours between runs, to vary the viscosity of the fluid and the sphere diameters, and to ensure very carefully controlled experimental conditions.

The solid symbols in figure 11 correspond to the 'zigzag' regime, in which the sphere oscillates periodically in a vertical plane. The vibrating trajectories shown in figures 3 and 9 are typical of this regime, throughout which we only found motion in a plane. Despite previous reports of 'spiralling' motion by Preukschat (1962), Shafrir (1965), and others, no spheres within the range of parameters studied in this map moved in a

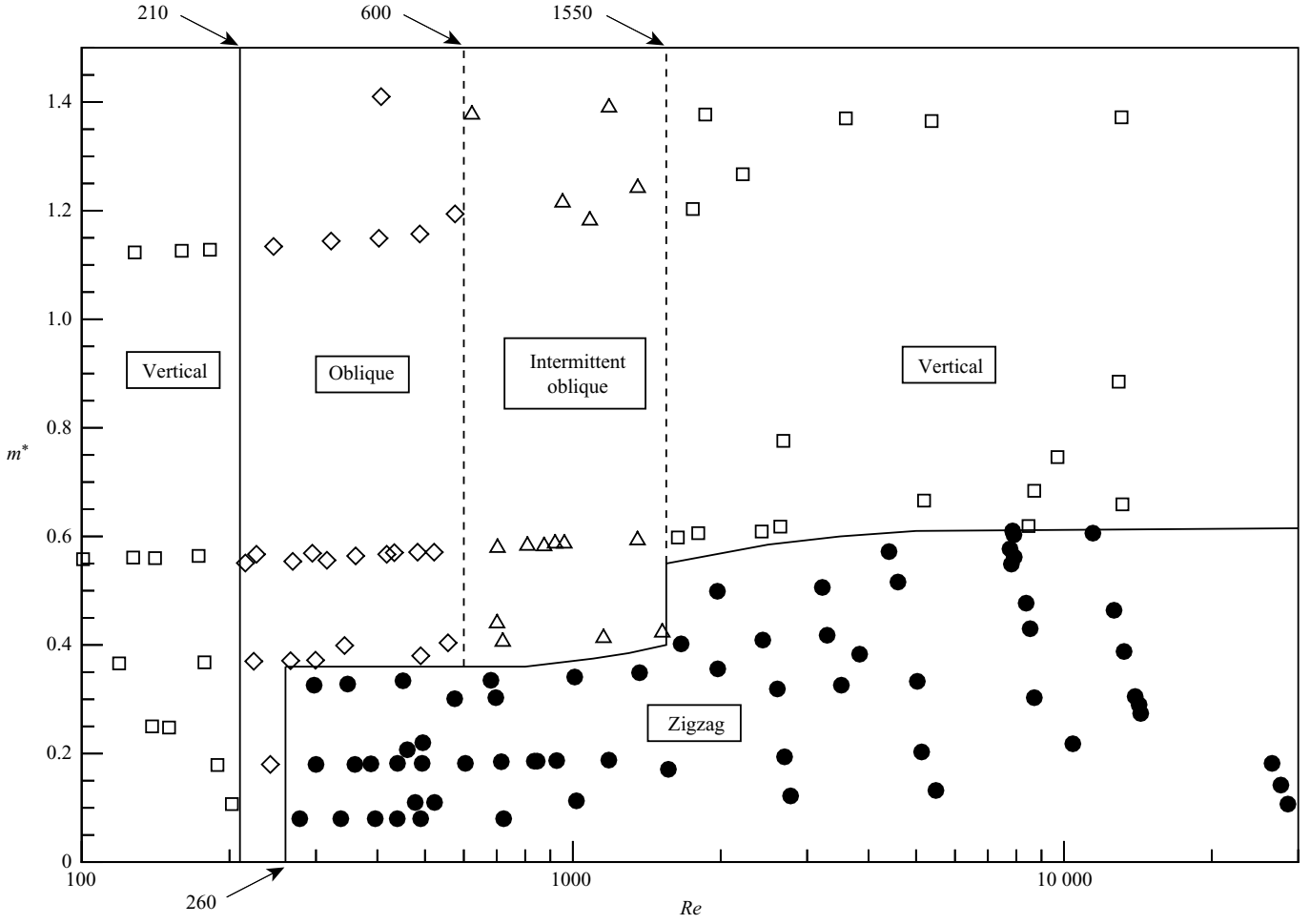

FIGURE 11. Map of regimes of sphere motion in the $\{m^*, Re\}$ plane.

helix. Amplitude and wavelength measurements for these experiments may be found in Appendix A.

When the sphere does not vibrate, there exist a number of possible regimes, depending on the Reynolds number. For $Re < 210$, the sphere rises vertically for all mass ratios, as might be expected, since the wake of a stationary sphere at these Reynolds numbers is axisymmetric. Following this vertical regime, spheres moving rectilinearly at $Re = 210$–600 have oblique trajectories, as in the cases shown earlier in in figure 9(*a–c*). Around $Re \approx 600$, the oblique motion becomes intermittent. The shape of these intermittent trajectories approaches the vertical more closely as the Reynolds number is further increased. At $Re = 1550$, the motion of the sphere becomes vertical and steady. The trajectories in figure 3(*a–b*) are typical of this regime. These transitions in the non-vibrating regimes are associated with changes in the wake of the sphere, which will be discussed in § 4.2.

In contrast to the results compiled from the variety of sources shown in figure 1, the present map shows a distinct boundary between spheres that vibrate periodically, and those that do not. The line separating the zigzag regime from the rectilinear ones indicates that the critical mass is approximately constant over two wide ranges of Reynolds number. Vibration first occurs at Re near 260, slightly less than the critical Reynolds number marking the onset of vortex shedding for a fixed sphere, $Re \approx 275$ (e.g. Sakamoto & Haniu 1990; Natarajan & Acrivos 1993). Over the range $Re = 260$–1550, the critical mass has a value just below 0.4. At $Re = 1550$, it jumps to $m^*_{crit} \approx 0.6$, where it remains until $Re \approx 15\,000$, the upper limit of our experiments.

It should be emphasized that in all the rectilinear regimes and for intermittent oblique trajectories, the motion never approaches the periodicity of the vibrating spheres shown in figures 3 and 9, even in a transient sense. Thus, there always exists a stark contrast between the vibrating and rectilinear regimes for the entire range of Reynolds numbers studied. We also observe this distinction from measurements of the mean drag coefficient, C_D, shown in figure 12. At all Reynolds numbers, the drag of spheres moving rectilinearly is nearly identical to the drag of a stationary sphere at the same Re, falling on the lower curve, from the data of Wieselsberger (1921) and Liebster (1927) compiled by Schlichting (1955). Vibration, however, results in a drag coefficient that is typically twice as large as the stationary sphere case (the upper curve). It should be mentioned that some of the variation of the drag of the vibrating spheres may be attributed to the effect of the oscillation amplitude. Where a larger degree of scatter exists, we find that lighter spheres, which tend to have higher amplitudes, consistently exhibit greater drag, so there is a trend underlying the apparent scatter. The relative clarity of this plot, exhibiting two clear regions, a low drag corresponding with the steady sphere motion, and the high drag condition for the zigzag trajectories, may be contrasted with the large scatter of data plotted earlier in figure 2 from collected previous results, where it was difficult to determine any regimes.

4. Wake patterns in different regimes of motion

In this section, we will explore the wake modes that correspond to the regimes of motion in the present map (figure 11). While the shedding of vortex loops has been identified in previous studies of the wakes of freely rising and falling spheres, there have been no descriptions of what periodic vortex formation modes may exist, especially when there are interactions between the body motion and vortex formation. We will show that the wakes of the rectilinear regimes tend to be similar to the wakes of fixed spheres, as might be expected. Vibrating spheres, however, exhibit a new

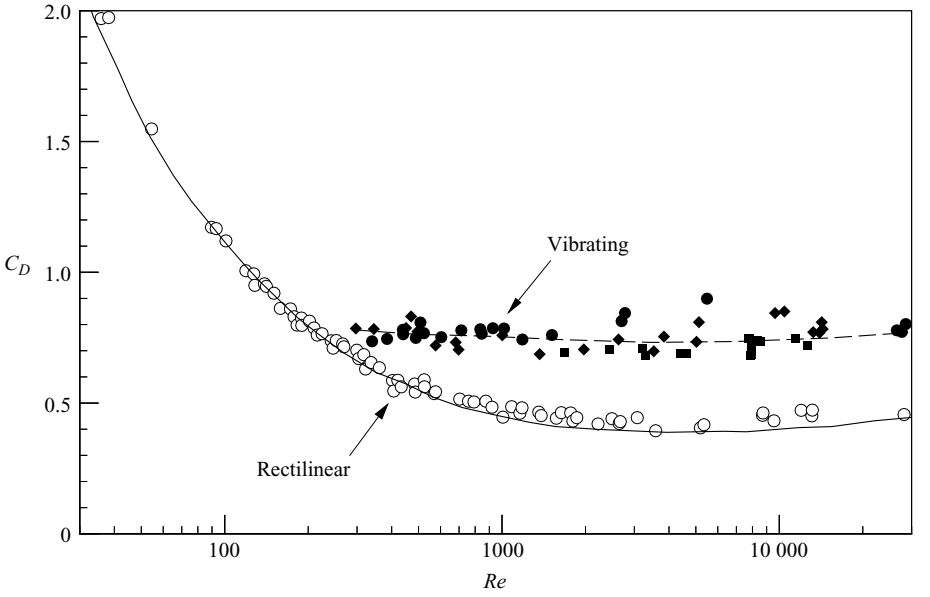

FIGURE 12. Mean drag coefficient for rising and falling spheres. The drag for spheres moving rectilinearly is approximately equal to the stationary sphere drag. Vibration causes a significant increase in drag. For $Re > 1550$, this increase tends to be higher for the lightest spheres, which have larger amplitudes. Vibrating spheres: ●, $m^* = 0.0-0.2$; ◆, $m^* = 0.2-0.4$; ■, $m^* = 0.4-0.6$. ○, rectilinear trajectory; —, drag for stationary sphere from Wieselsberger (1921) and Liebster (1927).

mode of vortex formation. The periodic vortex patterns that are observed will be classified by the number of vortex structures produced per wavelength.

4.1. *A new four-ring '4R' mode of vortex formation for rising spheres in zigzag motion*

The preliminary visualizations in figure 4(*b*), showed that for a vibrating sphere, four vortex structures are formed in each cycle of oscillation. The evolution of this wake as a function of time is shown in figure 13. Some of the structures here resemble vortex loops or rings, but it is difficult to describe them more precisely. Certainly the four structures (within a cycle) can be followed in time, and they are found to move upstream under their own induced velocity, indicating that they may perhaps represent vortex rings, although the dye marking each structure does not clearly indicate a ring. This difficulty in determining the structures clearly is partly due to the fact that the sphere used in this experiment had a diameter of only 0.2 cm, but was rising with a velocity of $20\,\mathrm{cm\,s^{-1}}$ (and partly due to the different diffusivities of the dye versus the vorticity). Such small sizes and high body velocities present a fundamental challenge for studies of the wakes of freely rising or falling spheres at low or moderate Reynolds numbers.

Our solution to this problem is to measure carefully the zigzag trajectory of a freely rising sphere $\{x(t), y(t)\}$, and use that trajectory as an input into a computer-controlled XY towing tank. In the towing tank, we can prescribe a trajectory identical to that of the rising sphere, but use a much larger body ($D = 3.81$ cm) towed at a significantly lower velocity ($U \approx 1\,\mathrm{cm\,s^{-1}}$), while maintaining the same Reynolds number. We need make no assumption of sinusoidal motion; we use whatever the measured trajectory yields. This novel technique, in this problem, greatly enhances the

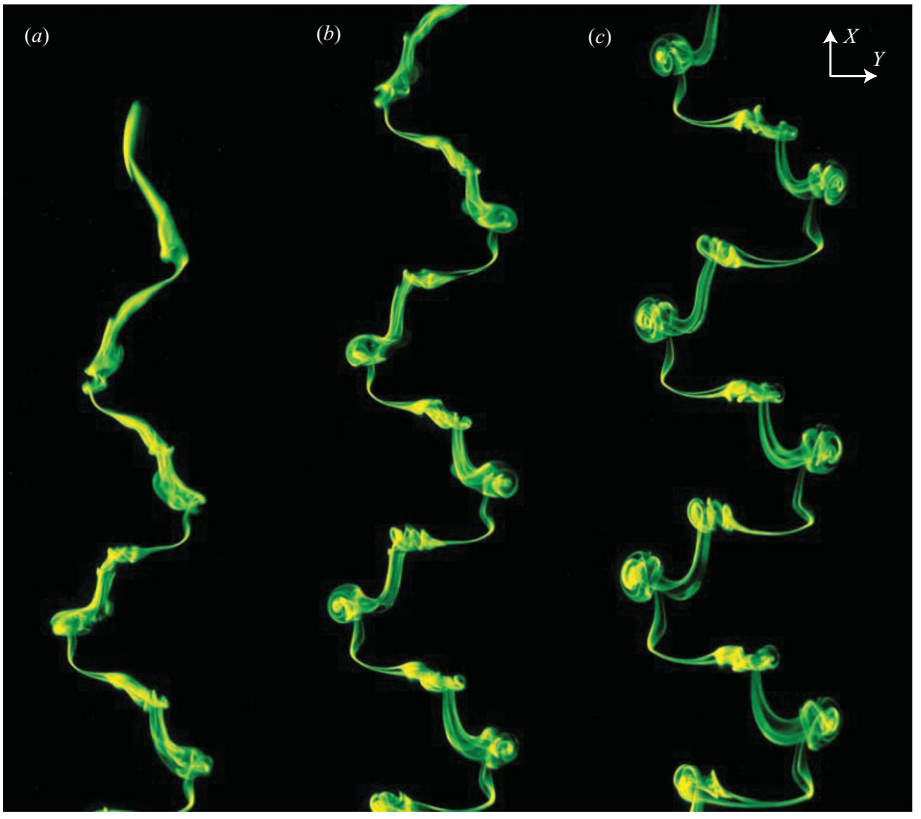

FIGURE 13. A new mode of vortex formation for a vibrating sphere comprising four vortex rings shed per cycle of oscillation. The sphere, located at the top of (*a*), has risen out of the frame in the next two images (*b–c*) taken approximately one and three periods ($t/T \approx 1, 3$) later. $m^* = 0.08$, $Re = 450$.

spatial and temporal resolution of our visualizations, allowing detailed visualization of the wake structures and their evolution, as well as measurements of vorticity. The effectiveness of using the towing tank is illustrated in figure 14, where we examine the structures formed in a single cycle of oscillation for a freely rising sphere, and for a sphere undergoing controlled motion. Despite the very different scales (typically 2 cm across the wake for the rising body, as opposed to 40 cm for the sphere in the XY towing tank), the pattern in both cases is identical, but the wake of towed sphere shows far more detail.

In this wake pattern, two structures are formed in each half-cycle: a larger, 'primary' structure near the peaks of the sphere motion, and a 'secondary' structure located near the centreline, labelled in figure 14. In figure 15, we focus on the evolution of the primary structure, viewed in a direction parallel to the Y-axis. Initially, the primary structure is shed as a vortex loop that rolls up from the sphere in figure 15(*a–b*). The legs of this loop comprise a counter-rotating vortex pair seen in figure 15(*c–d*). As the vorticity convects downstream relative to the body, the head of the loop begins to pinch off in (*e–f*), resulting in a structure which resembles a vortex ring, except that the two sides of the structure do not appear to reconnect fully.

To determine the evolution of the vortex structures accurately, vorticity measurements are needed, since the rate of diffusion of dye (with molecular diffusivity,

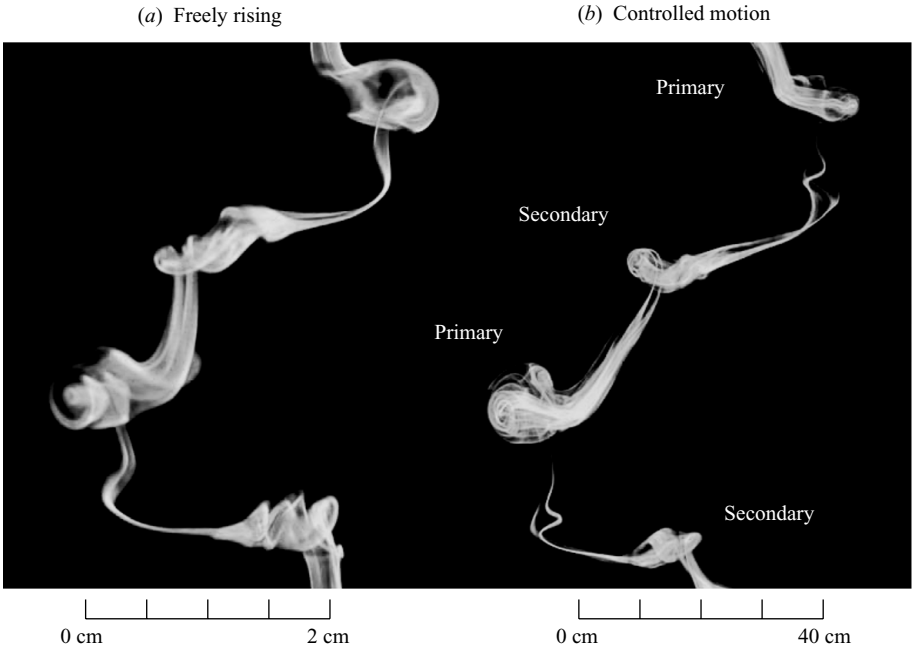

FIGURE 14. Comparison of the wakes of rising and towed spheres with identical motion. (*a*) Wake of a vibrating freely rising sphere, $m^* = 0.08$, sphere diameter = 0.2 cm. (*b*) Wake of a towed sphere controlled to move with the same trajectory, sphere diameter = 3.8 cm.

$\mathscr{C}$) and of vorticity are quite different here. The Schmidt number $Sc = \nu/\mathscr{C}$, relating these diffusion rates, is around 1200 (Quinn, Lin & Anderson 1986), meaning that the more rapidly diffusing vorticity may be present even where there is no dye. Employing PIV, we place the light sheet coincident with the $(X–Y)$ plane of symmetry (figure 16), passing through the region of the primary structure where no dye is visible. Despite the absence of dye between the vortex pair at the location of the 'pinch-off', our PIV measurements (figures 17 and 18) reveal the development of highly concentrated vorticity in this area. If we now look at figure 17, initially, the strength of the vorticity in the region with no dye is distinctly weaker, as in the region of red, anticlockwise vorticity at $X/D = 9$ (primary structure marked with a *). Further downstream, the circulation of the positive and negative vorticity regions (marked with a **) become approximately equal. At this point, the circulation around the entire primary structure is the same, as seen from additional PIV measurements in the $X–Z$ plane in figure 18(*a*), which confirm the formation of the ring.

In a similar manner, the secondary structure is created as the trailing vortex pair pinches off to form an additional vortex ring in each half-cycle, shown in figure 18(*b*). Preceding the formation of the secondary structure, the two counter-rotating streamwise vortices cross over one another. As they do so, they pass through the laser sheet and are visible in figure 17 between each primary structure and the secondary structure immediately downstream. This crossover provides a mechanism for the change in sign of the streamwise vortex pair as the body moves from one half-cycle of oscillation to the next.

It is the creation of the additional secondary structures that differentiates the present four-ring pattern from all previously observed sphere wakes, but thus far, it is unclear why the secondary structure occurs. With the ability to control the body motion

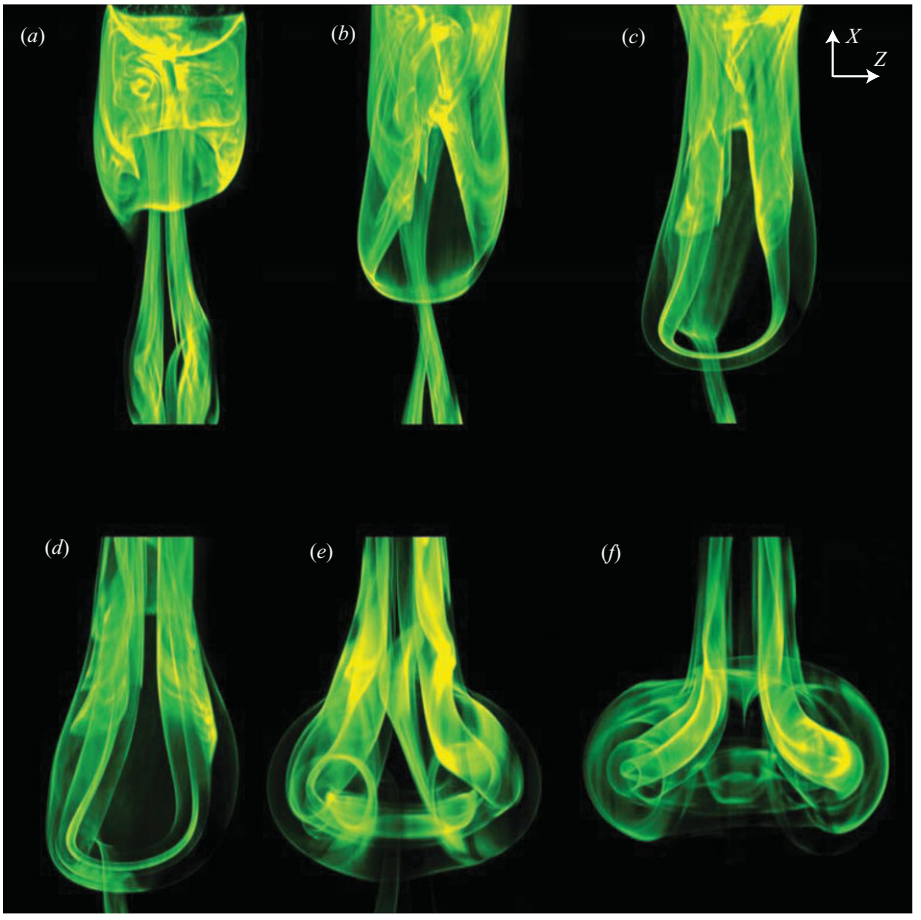

FIGURE 15. An enlarged view of the evolution of the primary structure, from a vortex loop into a vortex ring. The sphere, visible in (*a*), moves in the upward (+*X*) direction and vibrates normal to the *X*–*Z* plane (towards and away from the viewer). Images taken at times $t/T = \{0.0, 0.1, 0.2, 0.3, 0.5, 0.8\}$. $Re = 450$.

in a towing tank, it is possible to prescribe trajectories that differ slightly from the actual path of the rising sphere, and to study how these minor changes in the motion affect the wake. A feature of the oscillating sphere's motion that we observed from the Lissajous figures is the existence of streamwise vibration. The amplitude of streamwise vibration is quite small in this case, typically as low as $A_X^* = 0.04$, which corresponds also to an amplitude of the rising velocity of only about 3.6 %. Even though these levels of streamwise vibration are small, we ran an experiment for which the streamwise vibration is made equal to zero; we expected its influence to be negligible. Surprisingly, this small amount of streamwise vibration has a significant impact on the wake pattern. An image of the secondary structure for an experiment with streamwise vibration, is shown in figure 19(*a*). However, when A_X^* is set to zero (figure 19*b*), the secondary structure disappears. It appears that the secondary vortex ring is caused by the streamwise body vibration, sufficient to trigger the sensitive counter-rotating vortex pair to pinch off along its length midway between primary structures.

The four-ring mode of vortex formation found at $Re = 450$ persists throughout the regime of zigzag vibration. Its existence at higher Reynolds numbers is confirmed by

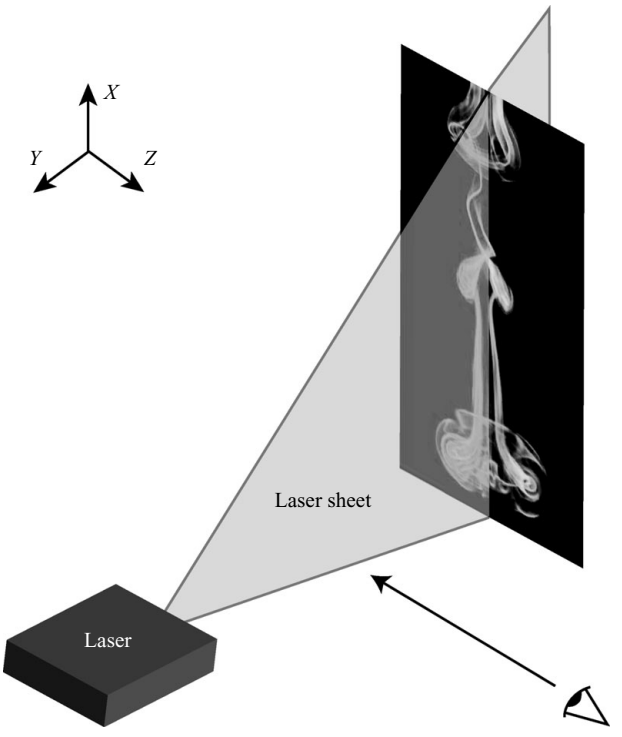

FIGURE 16. Schematic of PIV light sheet orientation to determine vorticity in the X–Y plane. The dye photograph is viewed from the Y direction, as in figure 15.

the dye visualizations and PIV for $Re = 6000$ in figure 20. As the Reynolds number is varied, a primary structure and a secondary structure are formed in each half-cycle, however, their relative spacing may differ with changes in the wavelength.

The process of pinching off and reconnection to form vortex rings that we have described here is similar to the one observed in other studies of the wakes of spherical bodies. The numerical simulations of Mittal (1999) and Mittal, Wilson & Najjar (2002) have provided evidence for the formation of vortex rings, originating as a single-sided chain of vortex loops in the wake of a fixed sphere at $500 < Re < 1000$. In the case of a tethered or elastically mounted sphere, measurements of vorticity by Govardhan & Williamson (2005) show a double-sided chain of vortex loops, which began to pinch off into rings. Magarvey & Bishop (1961*a*,*b*), in their dye visualization study for falling liquid drops, also found a double-sided vortex loop wake, evolving into what might be interpreted as two vortex rings per wavelength, a pattern which Goldburg & Florsheim (1966) reported that they observed for falling solid spheres. While the vortex rings in these other flow configurations are similar to the structures in the present pattern, fewer rings are formed per cycle. Since wake modes with various numbers of vortex rings are possible, a method of classifying these patterns may prove useful. Such a classification was developed for oscillating cylinders by Williamson & Roshko (1988), who, for example, defined two single vortices shed per cycle as the '2S' mode, and two counter-rotating vortex pairs as the '2P' mode. As new patterns for cylinder wakes were discovered, this terminology was easily extended, as in the case of two vortex triplets, a '2T' mode (Jauvtis & Williamson 2004), and of two co-rotating vortex pairs, a '2C' mode (Flemming & Williamson

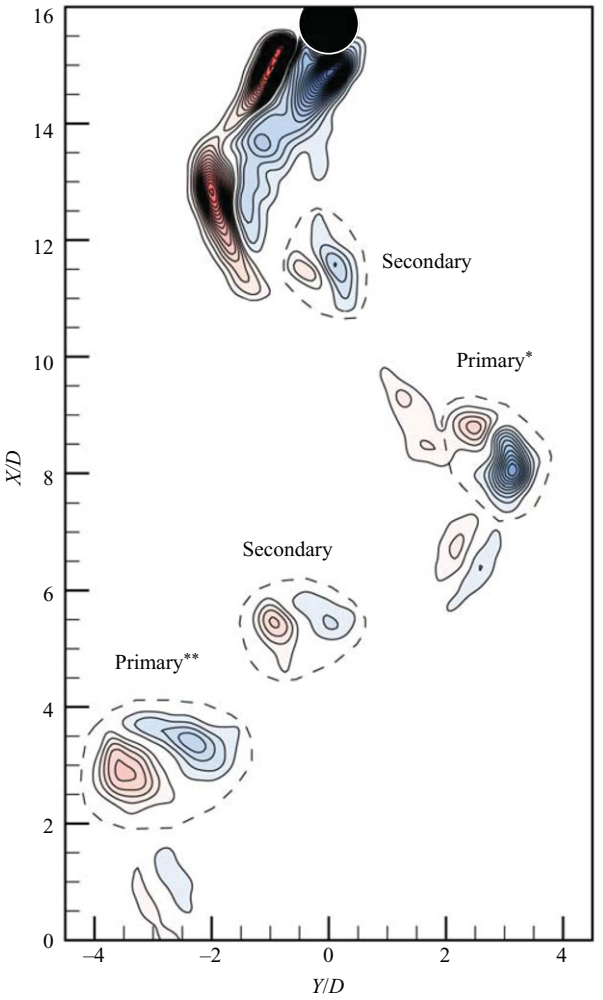

FIGURE 17. Vorticity measurements of the four-ring wake pattern for a vibrating sphere. The sphere, whose motion is controlled in a towing tank, is moving upwards and is located at the top of the image. Contours of vorticity are $\omega D/U = \pm\{0.15, 0.30, 0.45, \ldots\}$. $Re = 450$.

2005). Using similar nomenclature to Williamson & Roshko (1988), we will refer to the new four-vortex-ring wake mode for the rising sphere as the '4R' mode. Further periodic vortex patterns in this paper, similarly comprised of vortex rings, will also be defined according to this convention.

It should be noted that the only difference between the trajectories we prescribe in the towing tank and the motion of a rising sphere is that the freely moving body also has the ability to rotate. To examine the possibility of rotation, we considered two examples of vibrating spheres, at $Re = 450$ and at $Re = 10\,000$, both with $m^* \approx 0.33$. On the surface of these spheres, we drew a grid of latitude and longitude lines. From video of the sphere's motion, the movement of the gridlines allows the amount of rotation to be determined. For $Re = 450$, we observed periodic rotation with an amplitude of 14.7° in the Z direction (about an axis normal to the plane of vibration), acting over the same long wavelength as the transverse vibration ($\lambda^* \approx 14$). This amount of rotation corresponds to an angular acceleration, $\mathrm{d}\Omega/\mathrm{d}t$, with an amplitude of

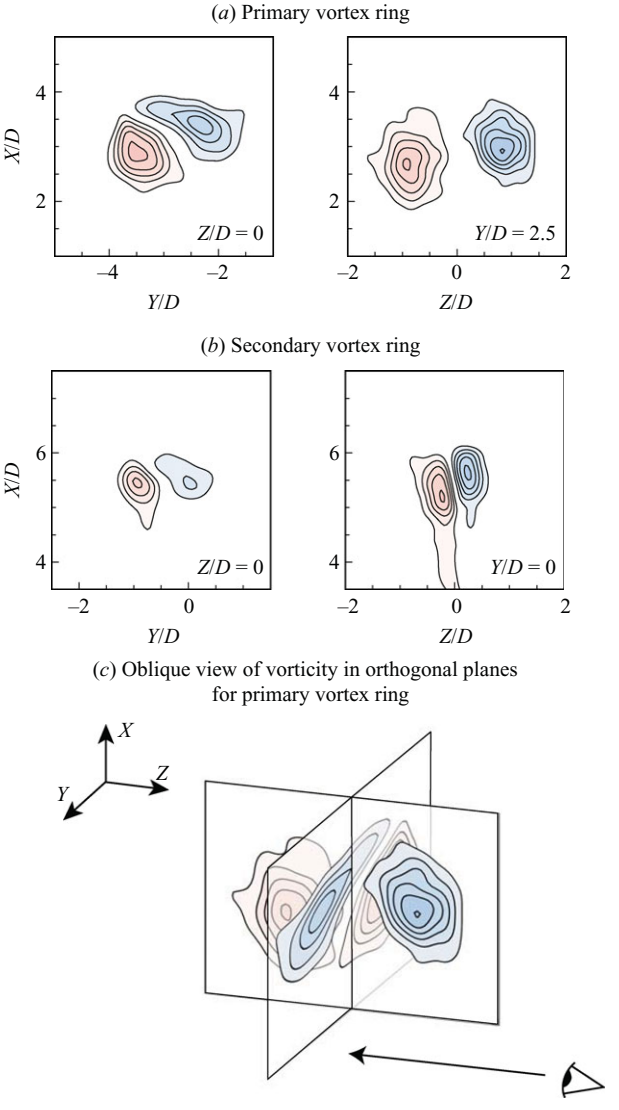

FIGURE 18. Views of the (*a*) primary and (*b*) secondary structures of the 4R mode in the X–Y and X– Z planes. (*c*) The two planar views of the primary structure in (*a*) are also arranged in three-dimensional space, with an orientation corresponding to the schematic in figure 16. Contours of vorticity are $\omega D/U = \pm\{0.15, 0.30, 0.45, \ldots\}$. $Re = 450$.

$73\,\mathrm{rad\,s^{-2}}$, occurring due to a torque, $T = J\,\mathrm{d}\Omega/\mathrm{d}t$, generated by the wake, where J is the moment of inertia (in the present case, $J = 2.9 \times 10^{-9}\,\mathrm{kg\,m^2}$). Normalizing our torque measurements according to

$$C_T = \frac{T}{\frac{\pi}{8}\rho U^2 D^3}, \tag{4.1}$$

yields $C_T = 1.8 \times 10^{-3}$. While this is larger than the torque computed by Bouchet, Mebarek & Dušek (2006) for a stationary sphere at $Re = 325$, $C_T = 4.9 \times 10^{-4}$, it is considerably smaller than the value for a zigzagging oblate spheroidal bubble

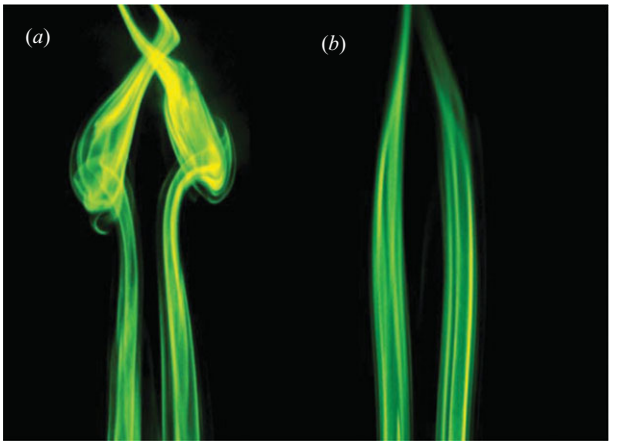

FIGURE 19. Dependence of the secondary structure on streamwise vibration. (*a*) Motion controlled to match exactly the measured rising sphere trajectory. $A^*_X = 0.04$. (*b*) The same motion, except streamwise amplitude set to $A^*_X = 0$. $Re = 450$.

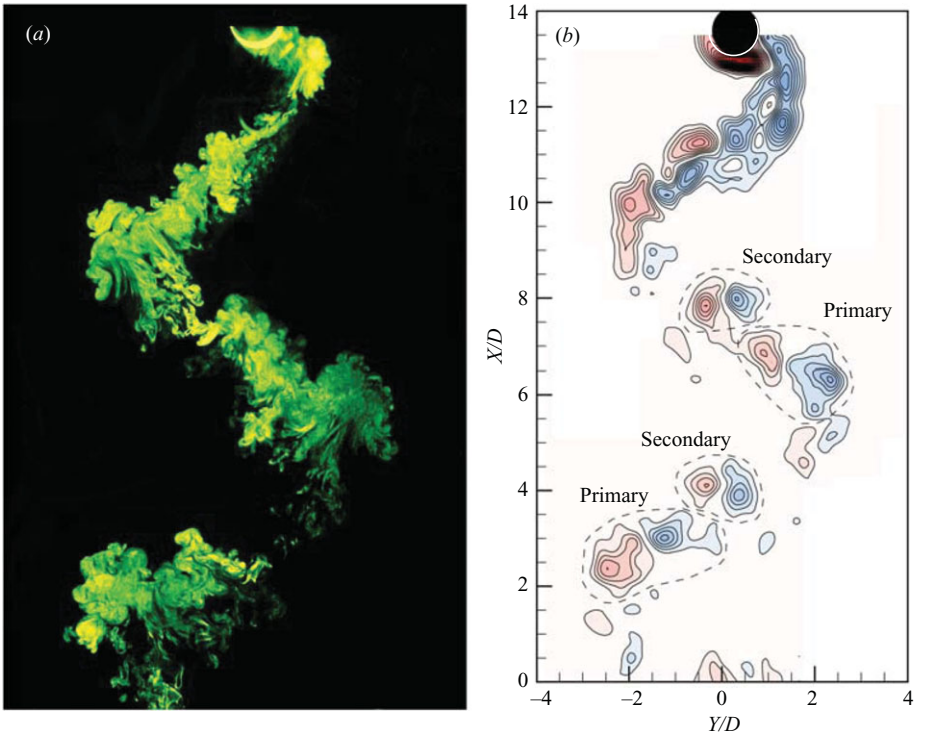

FIGURE 20. The existence of the 4R mode at turbulent Reynolds numbers ($Re = 6000$). Contours of vorticity are $\omega D/U = \pm\{0.1, 0.2, 0.3, \ldots\}$.

(Mougin & Magnaudet 2006), where $C_T = 5.9 \times 10^{-2}$ at $Re \approx 790$, $Ga = 390$. In the present case, the small torque and rotation rate suggest that the absence of a rotational degree of freedom for the towed body is unlikely to produce a significantly different wake than for the rising sphere, some confirmation of which is provided by the flow

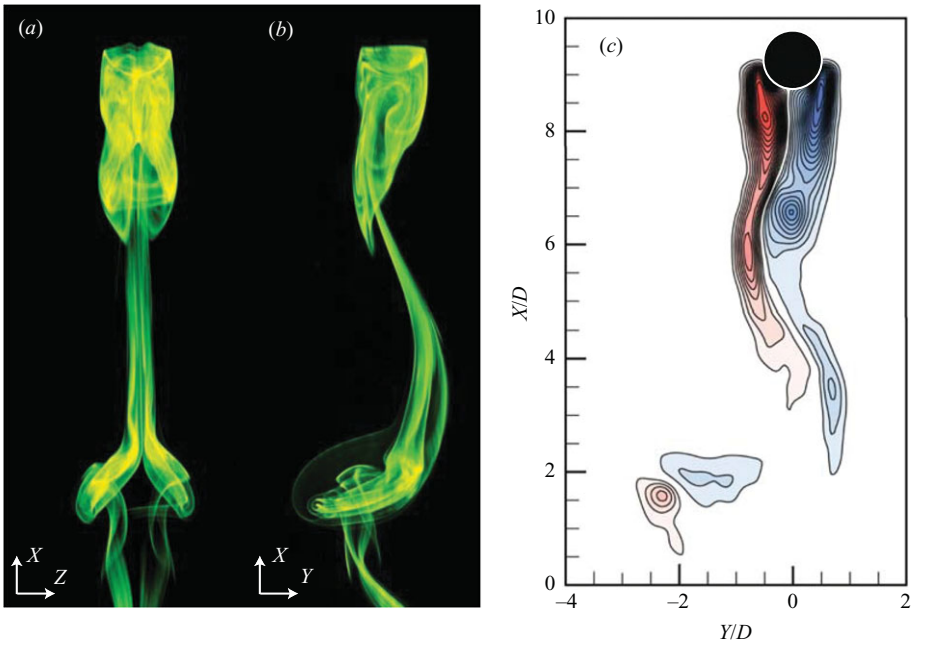

FIGURE 21. The R mode for the oblique regime. (*a–b*) Dye visualizations using laser-induced fluorescence (LIF) in the X–Y and X–Z directions. (*c*) Vorticity measurements from PIV. Contours of vorticity are $\omega D/U = \pm\{0.2, 0.4, 0.6, \ldots\}$. Motion controlled in a towing tank. $Re = 450$.

visualization results in the two facilities (figure 14). In the case of $Re = 10\,000$, we observe no measurable angular rotation of the sphere. It appears from our study that observable levels of rotation might only be found at lower Re.

4.2. *Wake modes for non-vibrating spheres*

Since their paths through the fluid are essentially in a straight line, the wakes of freely moving spheres with rectilinear trajectories should closely resemble those of spheres in a free stream. As such, the wakes of the fixed bodies will provide useful insight into the vortex dynamics of the freely moving bodies. For example, in the regime of vertical trajectories that exists below $Re = 210$, the fixed sphere wake is known to be axisymmetric (e.g. Natarajan & Acrivos 1993). The wake is therefore unable to exert any side force on the sphere to make it deviate from a vertical path. We will now consider the other non-vibrating regimes that occur as Reynolds number is increased.

The regime of oblique trajectories in figure 11 includes spheres of any mass ratio when the Reynolds number is between 210 and 260. This range roughly corresponds to Reynolds numbers where the wake of a fixed sphere is a counter-rotating vortex pair (Re = 210–275), which will produce a constant lift force in one direction transverse to the flow. When the body is unrestrained, this constant side force results in an oblique trajectory. After the onset of vortex shedding, a sphere in the oblique regime sheds a single-sided chain of vortex loops, shown in figure 4. Since the orientation of all the vortex structures is the same, a mean lift force on the sphere is generated, which has been measured for a fixed sphere with the same wake pattern by Johnson & Patel (1999). As shown by the PIV measurements in figure 21 for a towed sphere, the vortex loops develop into vortex rings, forming what we define as an ‘R’ mode, with one vortex ring formed per wavelength of wake formation.

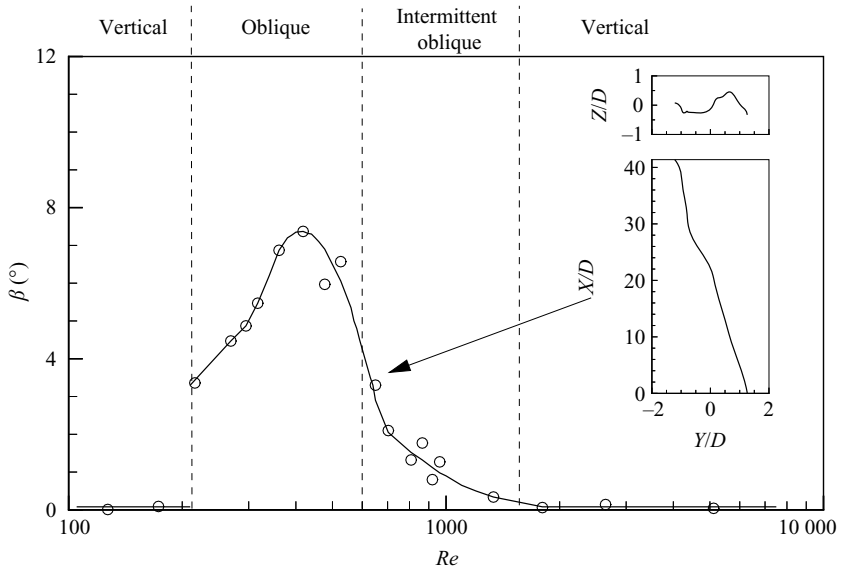

FIGURE 22. Variation in inclination angle of rectilinear trajectories with Reynolds number for spheres with $m^* > m^*_{crit}$. Beyond $Re \approx 450$, the angle of the oblique trajectories decreases rapidly, due to the irregular vortex shedding orientation. A typical trajectory is shown for the unsteady regime. $m^* = 0.55$–0.67.

Studies of fixed spheres indicate that this periodic vortex shedding continues until a Reynolds number around 420–500 (Sakamoto & Haniu 1990; Lee 2000; Tomboulides & Orszag 2000; Kim, Choi & Choi 2005), after which the vortices are shed with varying orientation. Simulations by Mittal *et al.* (2002) show that, at first, some preferred orientation of the shedding remains, but it diminishes as Re is increased. A similar phenomenon occurs for the freely moving sphere, and is suggested by the variation of the angle of the trajectories with Reynolds number (figure 22). At Reynolds numbers greater than around 600, the sphere path changes from oblique and rectilinear, to motion which is only intermittently oblique. This change is caused by the switch from the periodic 'R' mode, in figure 23(*a*) to a non-periodic mode in 23(*b*), where we find temporal variation of the orientation of the shed vortex rings. Increasing the Reynolds number in the intermittent oblique regime causes the shedding orientation to become more random (figure 23*b*–*c*), as it does for the fixed sphere. This trend resembles that of the fixed body, however, the Reynolds number at which it occurs is higher, $Re = 600$.

Although the regime of unsteady motion somewhat resembles the 'chaotic' trajectories described by Jenny *et al.* (2004) for $Re \approx 260$–550, there are several important differences. At the Reynolds numbers where Jenny *et al.* (2004) report that chaotic motion occurs, we only find oblique and zigzag trajectories, for which the wakes are periodic patterns of vortex rings. Only at higher Reynolds numbers, between 600 and 1550, do we find intermittent motion. Even then, the wake structure (figure 23*b*) in the intermittent oblique regime still appears to comprise a sequence of vortex loops evolving into vortex rings, consistent with the wake modes of a fixed sphere.

When the Reynolds number reaches 1550, the wake once again becomes periodic, with vortex rings being shed from alternate sides of the sphere, as shown for a

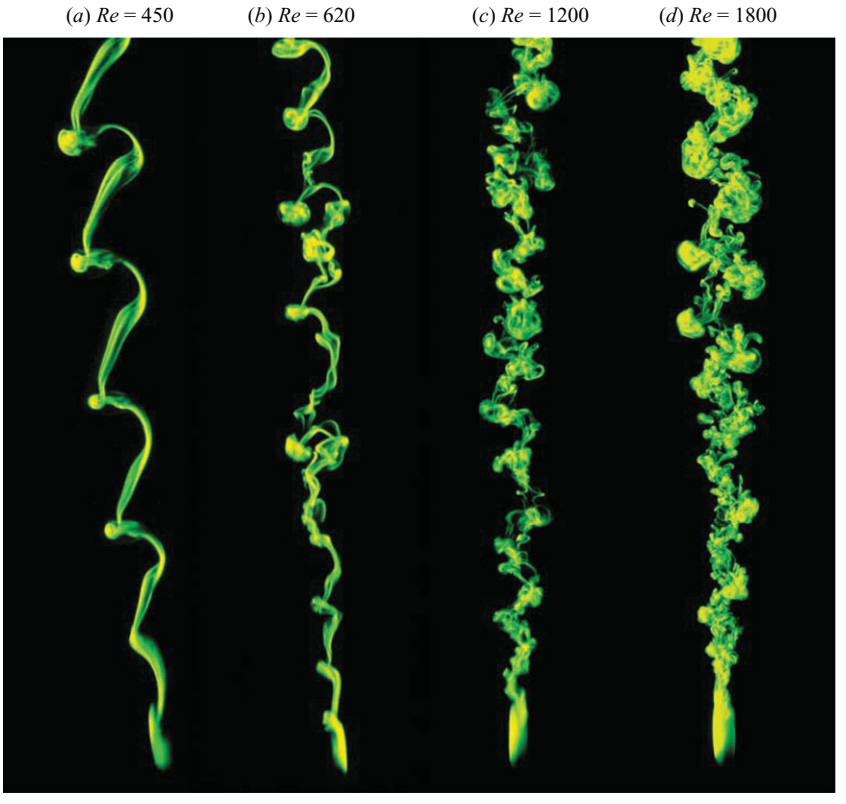

FIGURE 23. Wakes of freely falling spheres. (*a*) $Re = 450$. The periodic R mode occurs in the oblique regime. (*b*) $Re = 620$. In the unsteady regime, the orientation of shed vortex rings varies. (*c*) $Re = 1200$. The randomness of the wake in the unsteady regime increases with Re. Due to the absence of a strong preferred shedding orientation, the trajectory is essentially vertical. (*d*) $Re = 1800$. The wake changes to the periodic 2R mode.

falling body in figure 23(*d*) and for a towed sphere in figure 24 (which also includes some measurements of vorticity). The appearance of this periodic mode signals the beginning of a regime of vertical trajectories, and persists to the maximum Reynolds number studied here. There exist some differences in the reported Reynolds number at which the wake of a fixed sphere becomes a two-sided pattern. Sakamoto & Haniu (1990) state that it appears at $Re = 800$ in their experiments, considerably earlier than in the present study. However, simulations by Tomboulides & Orszag (2000) and Mittal *et al.* (2002) suggest that the 2R mode begins later. They find that the irregular shedding persists to at least $Re = 1000$.

The apparent transition at a Reynolds number of 1550 involves a jump in amplitude in the zigzag regime, and a jump in wavelength in the non-vibrating regime, as indicated by the plots and contours in Appendix A.

4.3. *Suggestion of a physical mechanism leading to the transition at* $Re = 1550$

The existence of a transition in the wake at $Re = 1550$ triggers a fundamental question: Why does the wake settle into a more periodic 2R two-sided vortex mode, yielding vertical sphere trajectories, at some particular Reynolds number? In other words, *is there some mechanism that encourages the wake to become more organized around* $Re = 1550$*?*

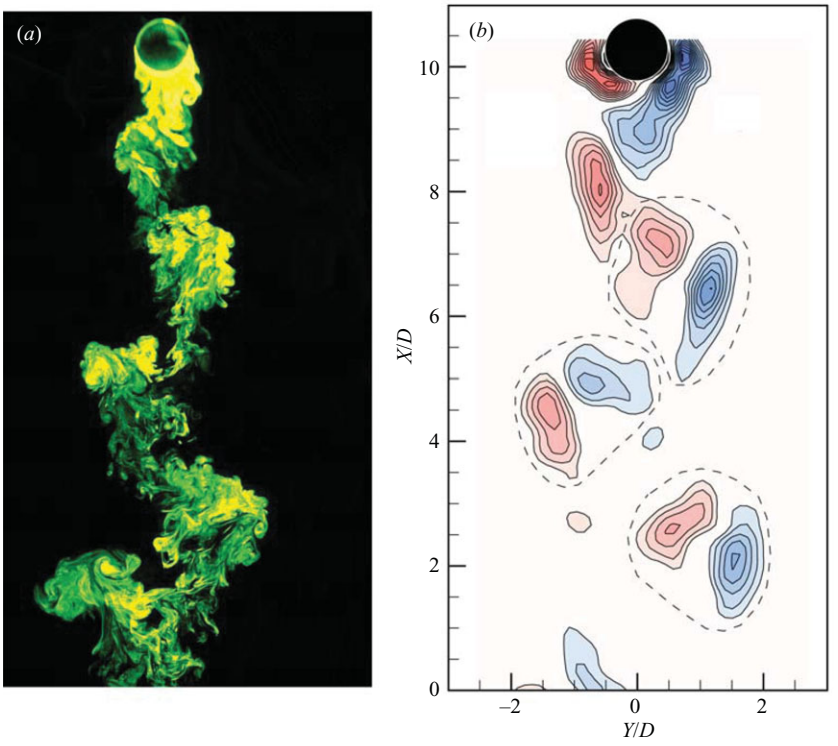

FIGURE 24. The periodic 2R wake mode for a sphere in controlled rectilinear motion. Contours of vorticity are $\omega D/U = \pm\{0.1, 0.2, 0.3, \ldots\}$. $Re = 6000$.

Since the sphere trajectories are straight and vertical, we naturally consider the fixed sphere wake. One should recall that there are two instabilities in the near wake of a sphere, just as there are in the cylinder wake (first highlighted by Bloor 1964). Not only is there an instability based on the dimensions of the body, in this case giving the low frequency of the vortex loops (f_{loop}), but there exists a 'Kelvin–Helmholtz' instability which develops in the separating shear layer coming off the sides of the body, giving a frequency f_{SL} for the instability waves. The latter instability scales on the typically thin separating shear layer thickness, giving a higher frequency than that for the vortex loops, $f_{SL} > f_{loop}$. Measurements of a higher frequency detected in the sphere wake have been made by Kim & Durbin (1988) and by Sakamoto & Haniu (1990), over a wide regime of Reynolds numbers. The point being made here is that it seems conceivable that the development of the more periodic 2R mode at around $Re = 1550$ could reflect an interaction between these two instabilities, a possibility that we now explore. Further research would be necessary to confirm the suggested ideas we now put forwards.

One might first consider the functional relationship between the shear layer frequency and the vortex loop frequency. To be brief, we follow the reasoning found in Bloor (1964), and also in Prasad & Williamson (1997), for the cylinder wake, where it is suggested that the shear layer frequency will scale on the velocity near the separation point, and the thickness of the separating shear layer (laminar boundary

layer), which yields

$$\frac{f_{SL}}{f_{loop}} \sim Re^{1/2}, \tag{4.2}$$

which is equivalent to what Bloor (1964) put forwards for the cylinder instabilities. This frequency ratio of the instabilities was revisited by Prasad & Williamson (1997) for the cylinder wake, and by noting that in fact the instability scales on the free shear layer thickness downstream of the body (as well as other considerations) they were able to deduce a power law, which actually fit the compiled data of almost all previous investigations much closer than the classically assumed 0.5 power law:

$$\frac{f_{SL}}{f_K} = 0.0235 \times Re^{0.67}, \tag{4.3}$$

where in this case f_K is the Kármán vortex frequency. Such an analysis for the sphere has not been performed, despite the fact that extensive frequency measurements for the instabilities have existed for 20 years.

We have therefore digitized the shear layer frequency and loop frequency data sets from the papers of Kim & Durbin (1988) and Sakamoto & Haniu (1990), and approximately deduced the ratio between instability frequencies, plotting the results in figure 25. We now find a new power law fit to all the data

$$\frac{f_{SL}}{f_{loop}} = 0.0050 \times Re^{0.83}. \tag{4.4}$$

Such an instability frequency relation has not been deduced before for the sphere.

This relationship may also relate to the incipience of the 2R mode around $Re = 1550$, and the existence of our regime boundary shown in the map of sphere vortex modes. If we look now at figure 25(b), we find that the Reynolds number where the shear layer frequency is double the loop frequency is given by $Re \approx 1350$,

$$\frac{f_{SL}}{f_{loop}} \approx 2 \quad \text{at} \quad Re \approx 1350,$$

which is of the same order as the Reynolds number for the incipience of the periodic 2R mode $Re = 1550$. It seems conceivable that in this regime of Reynolds number, there is a resonance between these two vortex instabilities, which would have the effect of providing more order, and more periodicity, to the otherwise more intermittent vortex loop formation. In our case here, free stream turbulence may contribute to the uncertainty concerning the Re where the two-sided vortex loop mode has been reported.

Physically, a resonance of the two instabilities could be imagined as follows. An evolving vortex loop on one side of the sphere wake close to the body would represent (as far as the shear layer instability is concerned) the formation of one shear layer vortex (which would initially take the form of a vortex ring around the near wake of the sphere). By symmetry, in the next half-cycle, one expects the next opposite signed vortex loop to evolve from another shear layer vortex (or the next vortex ring close to the body). For this phenomenon to occur, the frequency ratio is necessarily: $f_{SL} = 2f_{loop}$. Of course, this is only a suggested mechanism for the transition to organized vortex formation at $Re \sim 1500$, but it seems conceivable that a resonance might occur.

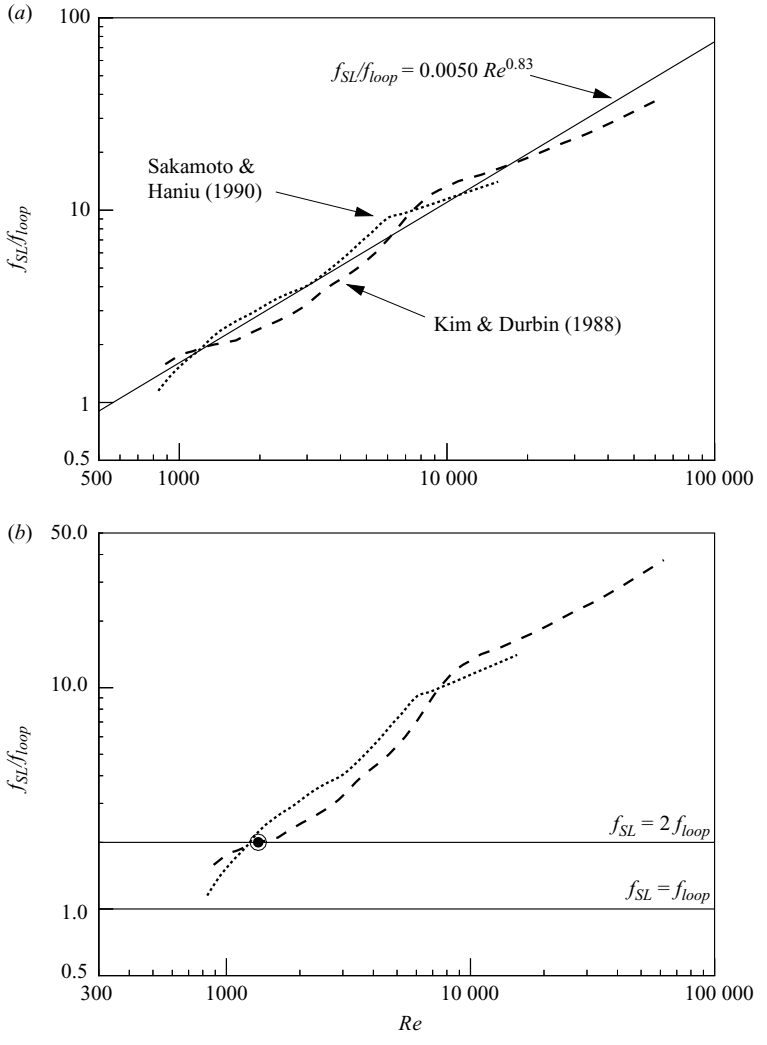

FIGURE 25. The ratio of the shear layer and vortex loop frequencies for a fixed sphere. (*a*) The normalized shear layer frequency is estimated as $f_{SL}/f_{loop} = 0.0050 \times Re^{0.83}$, from a best-fit to the frequency data of Kim & Durbin (1988) and Sakamoto & Haniu (1990). (*b*) The frequency of shear layer vortices becomes twice the frequency of shed vortex loops around $Re = 1300$. The proximity to the Reynolds number where the 2R mode appears for a falling sphere, $Re = 1550$, suggests that the onset of the 2R mode may be associated with a resonance between the shear layer and vortex loop frequencies.

5. Zigzag trajectories, helical motions and background disturbances

It should be pointed out that careful control of experimental conditions is essential in order to observe the dynamics described in this paper, in particular the rectilinear regime for rising spheres, which we shall now illustrate here. A central point is that we find spheres, with mass ratios somewhat greater than the critical value, are sensitive to small disturbances in the fluid, which can induce large non-periodic motions. In our study, we conclude that the disturbances in the fluid can be minimized by using a large settling time between experiments (at least 2 h) to allow the fluid in the tanks to become closely quiescent.

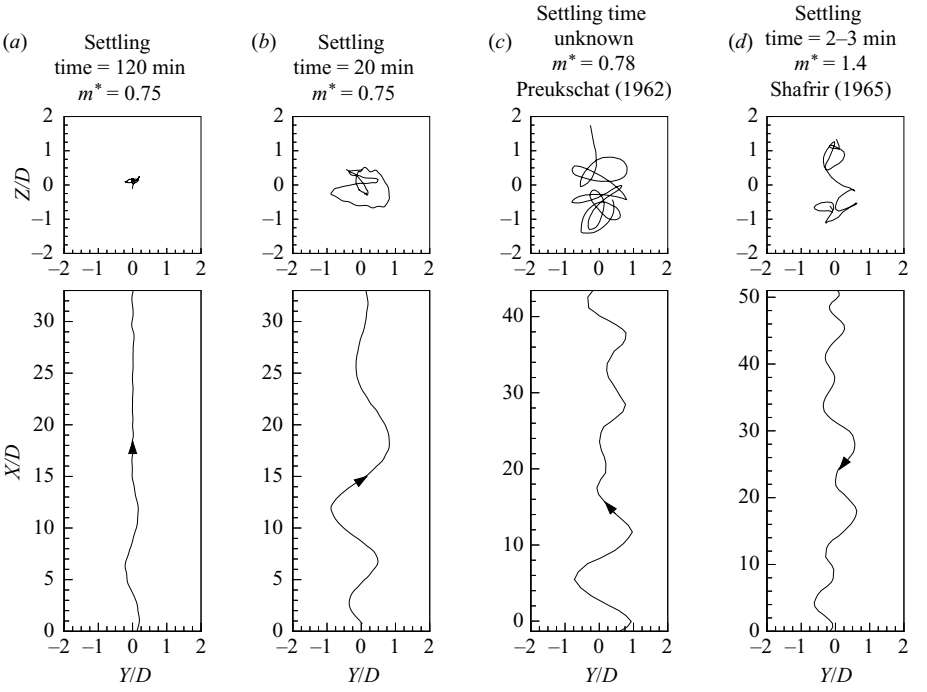

FIGURE 26. Effect of settling time on sphere motion. (*a*) Settling time = 120 min. The sphere rises rectilinearly through the quiescent fluid, following a brief transient. (*b*) Settling time = 20 min. Disturbances remaining in the fluid induce large random transverse motions. The same sphere was used for both experiments. $m^* = 0.75$, $Re = 9500$. (*c*) Settling time unknown (Preukschat 1962). $m^* = 0.78$, $Re = 6000$. (*d*) Settling time = 2-3 min. (Shafrir 1965). $m^* = 1.4$, $Re = 6000$.

As an illustrative example at this point, we observe the case of a rising sphere in the vertical rectilinear regime in figure 26(*a*), where the fluid is given the customary 2 h to settle. Following an initial transient that is quickly damped out, the sphere rises vertically. However, when the settling time is reduced to 20 min, we find considerable irregular motion throughout the rising trajectory in figure 26(*b*), presumably as the sphere is affected by disturbances in the fluid. These motions, however, are non-periodic, which is especially apparent when viewing from the top of the tank. The high degree of periodicity for the regular zigzag regime (illustrated for example in figure 9) indicates that any irregular motions due to a low and insufficient settling time, as shown in this example here, are quite distinct from (and should not be mistaken for) zigzag vibrations.

This result also suggests that one would not expect to find evidence of rectilinear trajectories for rising spheres if a low settling time is used. Indeed, our irregular motion (found for low settling times) appears qualitatively similar to several trajectories from previous studies that were classified as vibrating, even though the mass was higher than the critical values measured in this paper. One example is the path of an often quoted 'spiralling' sphere ($m^* = 0.78$, $Re = 6000$) from Preukschat (1962), shown in figure 26(*c*). The settling time for this experiment is not specified, and it is only stated that 'spheres were released one at a time'. Similarly, Shafrir (1965) reports 'slightly corkscrew' trajectories for his experiments using falling spheres, like the one in figure 26(*d*), where he allowed 'usually 2–3 min' for the water to settle. The resemblance

between these trajectories and our case with low settling time suggests that the amount of time between experiments may account for previous reports of vibration for spheres substantially heavier than the critical mass reported here, and would largely explain the disagreement amongst the reports of body dynamics discussed in the Introduction.

We also note that the trajectories of Preukschat (1962) and Shafrir (1965) are not spiralling. These apparently random motions are distinctly different from the nearly perfect spiralling paths of rising bubbles (Mougin & Magnaudet 2002; Wu & Gharib 2002). To our knowledge, there has been no clear evidence in the literature for spiralling or helical trajectories for rising or falling solid spheres. One might suggest that such helical motions (for $Re > 270$) would not be compatible with the induced fluid forces coming from unsteady vortex loops and rings shed from the sphere, since such a wake may not be able to provide the steady centripetal force required for a spiralling path.

6. Concluding remarks

In the present paper, we study the body dynamics and vortex wake patterns of spheres rising or falling freely through a fluid. Despite the number of studies that have considered this problem, beginning with Newton (1726), the fundamental question of when a rising or falling sphere will vibrate has not been clearly answered. Previous works have been confined to limited ranges of mass ratio and Reynolds number, and there clearly exists some disagreement as to when vibration occurs, and what types of motion exist. In this work, we systematically define the regimes of body motion and vortex wakes, over a wide range of mass ratio (m^*) and Reynolds number (Re), for the first time. We also measure the sphere drag, which is of course related to the modes of body dynamics.

Perhaps the most fundamental question that may be asked is: *when will a rising or falling sphere vibrate?* While addressing this question, we demonstrate the existence of a critical mass ratio, below which there is a regime of highly periodic zigzag vibration, and above which spheres move essentially rectilinearly, either vertically or at some oblique angle to the vertical. Initially, we illustrate two cases in detail, one for a low Reynolds number (450) exhibiting laminar wake flow, and one for a higher Re (10 000), involving turbulent wake flow. We find the critical mass ratio for $Re = 450$ to be $m^*_{crit} = 0.36$, and for the higher $Re = 10\,000$, we find $m^*_{crit} = 0.61$. Thus, there is clearly some influence on the critical mass coming from Reynolds number, as one would expect. These values are typical of two wide regimes of Reynolds number, within which the critical mass remains reasonably constant, as follows:

$$m^*_{crit} \approx 0.4, \quad Re = 260 - 1550,$$
$$m^*_{crit} \approx 0.6, \quad Re = 1550 - 15\,000.$$

In contrast to previous studies, in which vibration, either periodic or 'chaotic', is reported for all buoyant spheres (where $m^* < 1$), we find that there always exists *a wide regime of mass ratios for which rising spheres ascend without oscillation.* The existence of rectilinear motion for a regime of rising spheres, corresponds well with predictions of the critical mass based on previous vortex-induced vibration experiments with elastically mounted spheres.

In order to define the various dynamics and wake modes that exist for rising and falling spheres, we study 133 different combinations of Reynolds number and mass ratio, for which we perform nearly 690 experimental runs. One of the principal results of this work is the map of regimes of motion and vortex dynamics we present in figure 27, here in this section. At the lowest Re, all spheres move vertically, with

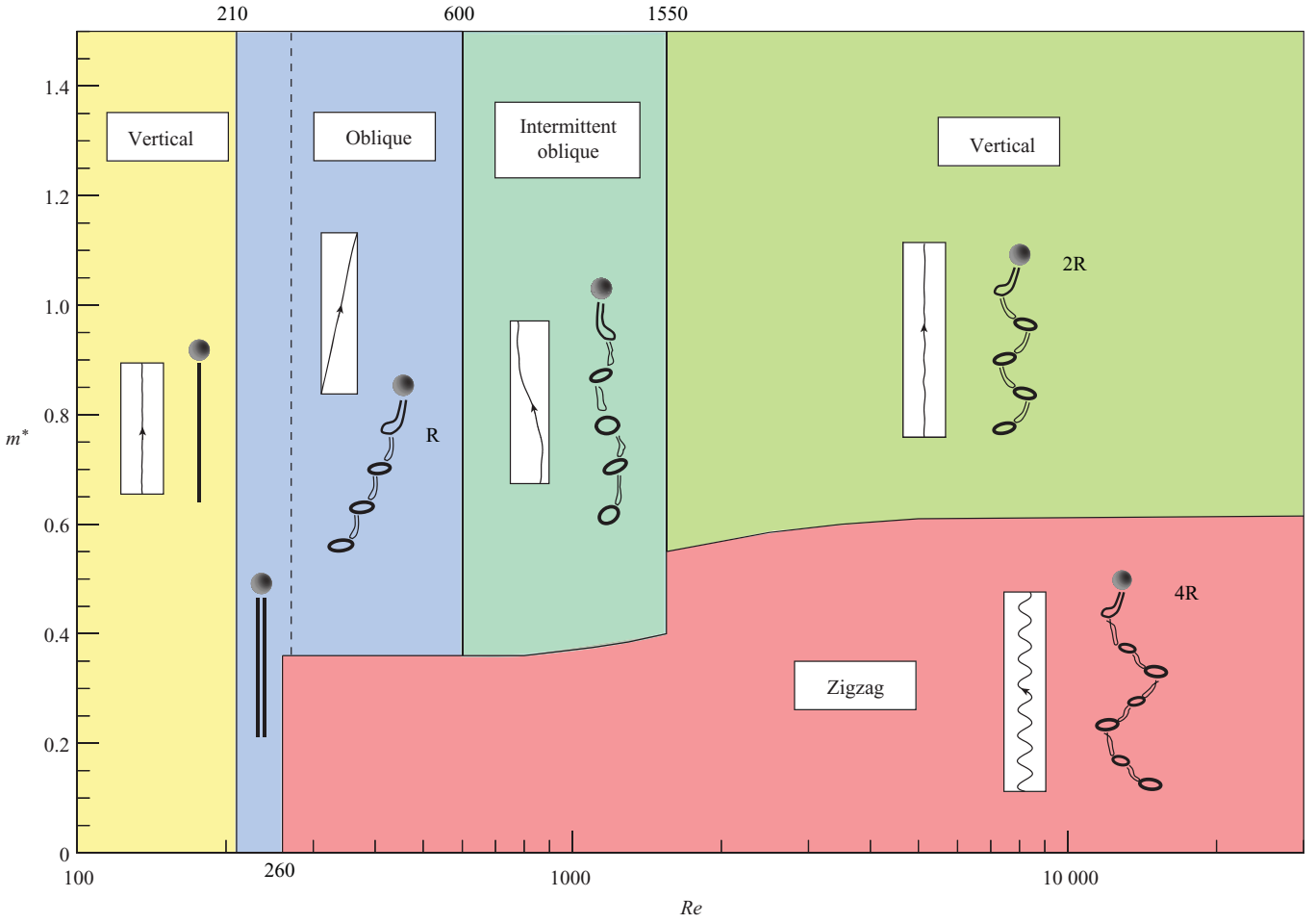

FIGURE 27. Map of regimes of sphere motion and associated wake patterns in the $\{m^*, Re\}$ plane. Typical trajectories are shown for each regime.

an axisymmetric wake. As the wake changes to a trailing vortex pair at $Re = 210$, it produces a steady side force on the body, which causes the sphere to move at some oblique angle to the vertical. The character of the body motion first becomes dependent on the mass at $Re = 260$, when spheres lighter than $m^*_{crit} = 0.36$ begin to vibrate. The periodic zigzag motion for these bodies corresponds to the discovery of a '4R' wake formation mode, comprising four vortex rings formed in each cycle of body motion. The critical mass remains fairly constant until we observe several distinct changes to the wake and dynamics at $Re = 1550$, after which the critical mass jumps to a value $m^*_{crit} \approx 0.6$. The vortex wakes of spheres with zigzag trajectories, in this turbulent wake regime, continue to exhibit principally the '4R' vortex wake pattern.

In the case of heavier spheres above the critical mass ($m^* > m^*_{crit}$), over the regime $Re = 270$–600, we find trajectories at some oblique angle to the vertical, shedding a single-sided chain of vortex rings, which we define as the 'R' mode. Beyond $Re = 600$, the oblique motion becomes intermittent, whereby the vortex rings in the body wake are shed with different orientations, becoming increasingly irregular as Re increases further. However, as noted also for the light spheres, there is a transition Reynolds number of 1550, beyond which the shedding mode for heavier spheres changes to the periodic '2R' mode, comprising a double-sided chain of vortex rings (i.e two vortex rings formed per cycle of body motion).

The structure of these periodic shedding modes are obtained using both dye visualizations, and vorticity measurements using PIV. It is only by using a technique of precisely replicating the motion (and matching the Reynolds number) of freely rising and falling spheres using a computer-controlled XY towing tank that we are able to study these wakes with much higher spatial and temporal resolutions. However, it is still difficult to visualize the three-dimensional structure of these wake patterns from two-dimensional images. We therefore now display the structure of the wakes using three-dimensional renderings of each mode. In the case of the 4R mode, the position of the streamwise vortex filaments is determined from dye visualizations, as illustrated by figure 28. The vortex rings, whose evolution is not captured fully by the dye, are defined with the help of vorticity fields from PIV (their size and orientation are approximately based on the contour of vorticity $\omega D/U = \pm 0.2$). We now employ the same approach to visualize, in figure 29, the three-dimensional structure of all three modes in the family:

$$\{R,\ 2R,\ 4R\}.$$

Obviously, a full measurement of vorticity, throughout a large volume of fluid simultaneously, would render a more accurate family of wake pattern images, but the approach here represents the principal features of the three vortex modes in the family.

Finally, in this paper, we have been able to collapse the drag force measurements onto two approximate curves when plotted as a function of Reynolds number. The lower drag curve corresponds with the rectilinear trajectories, while the other curve with the markedly higher drag represents the zigzag regime of body oscillation. This collapse of data is possible in the presence of minimal background disturbances, which has an effect on the body dynamics, and in turn, as noted by Newton in 1726, has a distinct effect on the mean speed of the sphere, and thereby its drag.

The support from the Ocean Engineering Division of ONR, monitored by Dr Tom Swean, is gratefully acknowledged (ONR Contract No. N00014-04-1-0031 and N00014-07-1-0303). The authors would also like to thank Tim Morse and for his extremely helpful input to this research, Paolo Luzzatto Fegiz for his expertise and

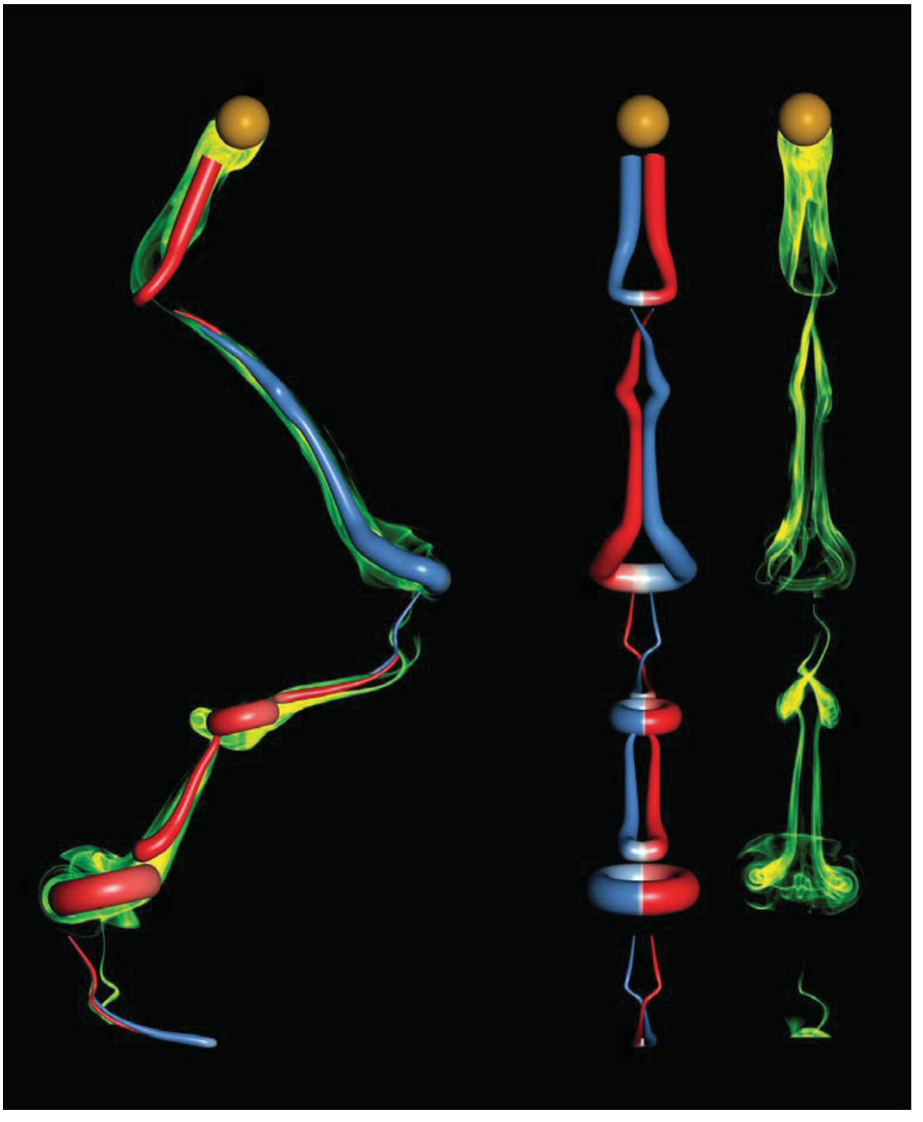

FIGURE 28. Creation of a three-dimensional rendering of the 4R mode. The positioning of the streamwise vorticity structures is determined from the dye visualizations. The location and size of the vortex rings are based on data from PIV measurements, and approximately represent the vorticity contour $\omega D/U = \pm 0.2$. The colour corresponds to the initial sign of the streamwise vorticity component: positive vorticity is shown in red, negative vorticity is shown in blue.

Chris Pelkie for his enthusiastic help in performing the three-dimensional image analysis.

Appendix A. Amplitude and wavelength measurements for rising and falling spheres

In Appendix A, we present further detailed measurements defining the sphere trajectories as a function of Reynolds number and mass ratio. One central purpose in providing this detailed data is to make clear that the transition at $Re \sim 1550$ is a

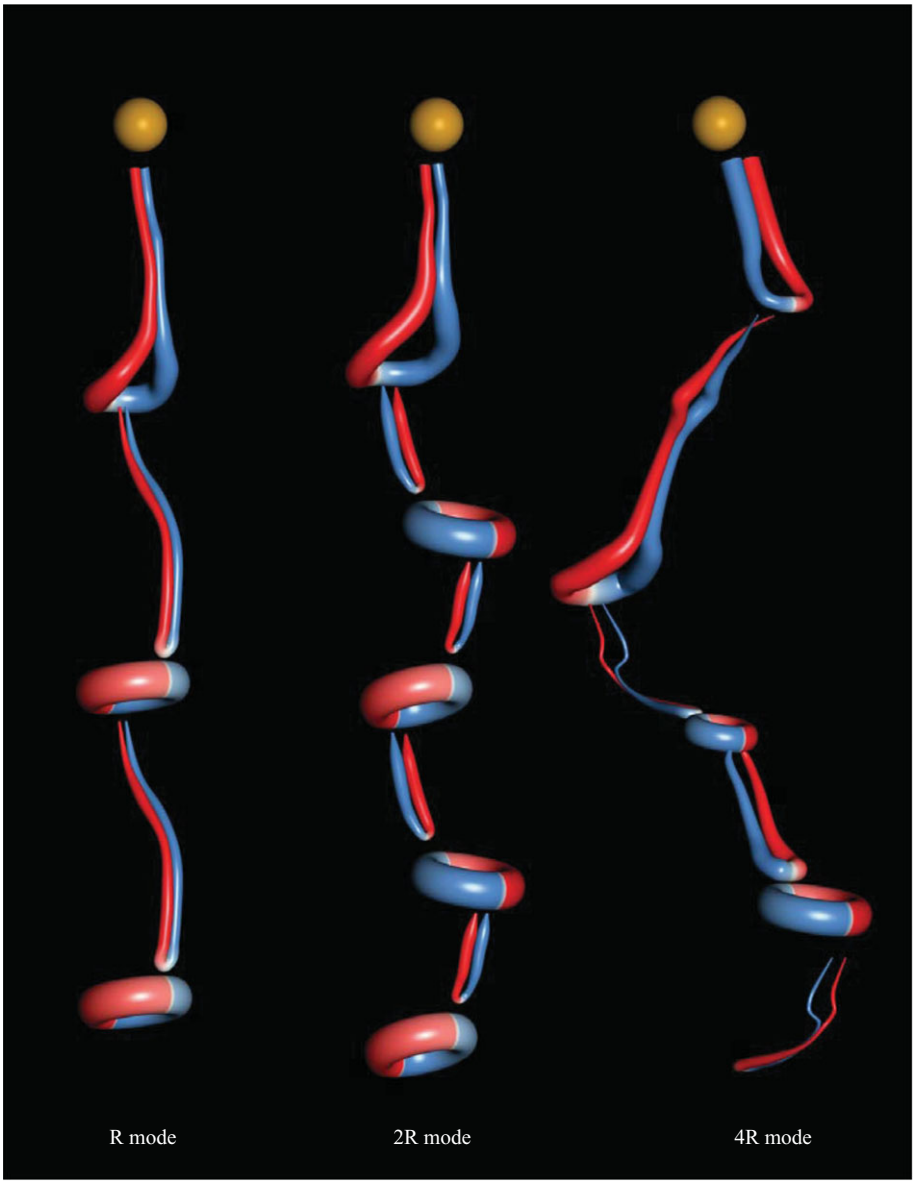

FIGURE 29. The family of periodic wake modes for rising and falling spheres. These three-dimensional visualizations are created following the approach shown in figure 28.

real phenomenon. We focus on the transverse amplitude, A_Y^* and the wavelength of the trajectory λ^* for spheres in the zigzagging regime, and also include measurements of the streamwise amplitude A_X^*.

We present the amplitude, wavelength and phase (between the transverse and streamwise oscillations) for a vibrating sphere in figure 30, where we have chosen mass ratios: $m^* = 0.30{-}0.38$. This may be considered a (nearly) horizontal cut through our map of regimes in figure 11, in contrast to the amplitude plots used to determine the critical mass (e.g. figures 6 and 8), which correspond to vertical (constant Re) cuts through the parameter space. Two spheres with different diameters are studied, with

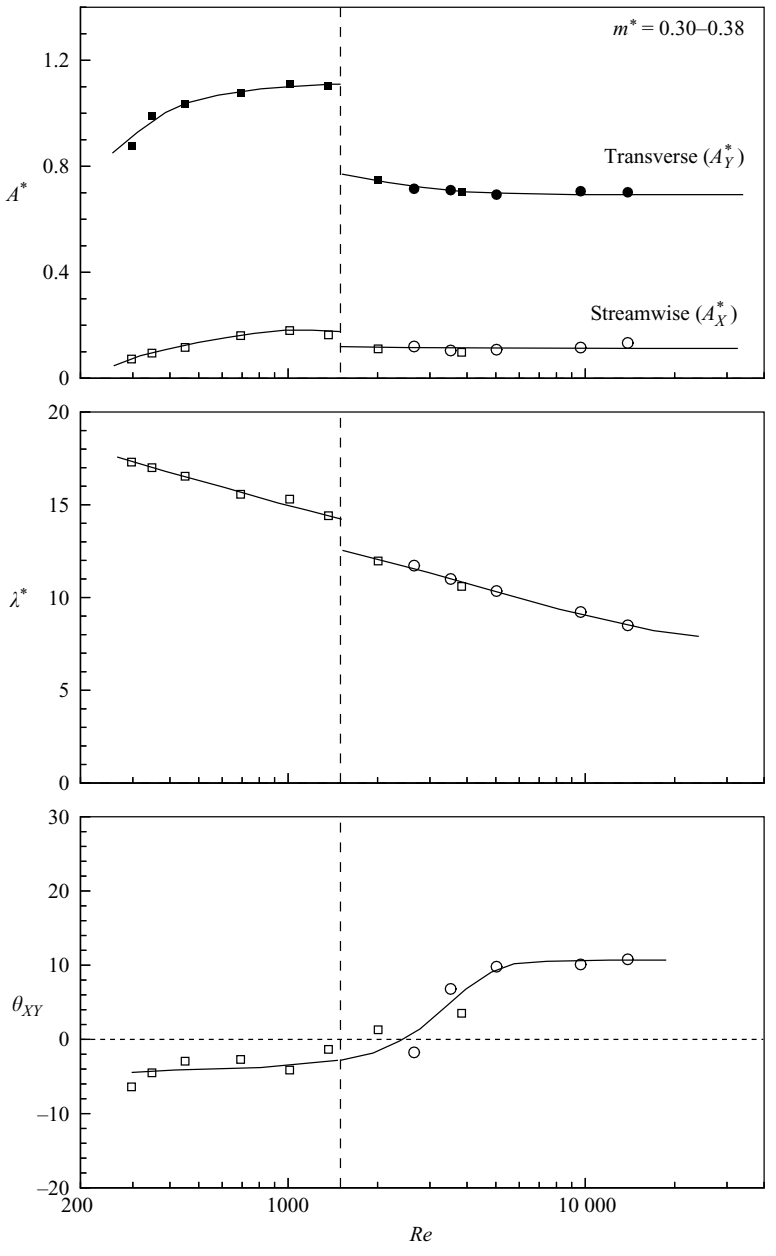

FIGURE 30. Variation of transverse amplitude (A_Y^*), streamwise amplitude (A_X^*), wavelength (λ^*) and phase (θ) with Reynolds number for (approximately) constant mass ratio. Distinct jumps in the amplitude and wavelength occur when $Re = 1550$ is crossed. Two different spheres were used: ■, □, $D = 1$ cm, $m^* = 0.32$–0.38; ●,○, $D = 2$ cm, $m^* = 0.30$–0.34.

the Reynolds number being varied by changing the concentration of a glycerin-water mixture (which results in a small increase in mass ratio as Re increases, yielding $m^* =$ 0.32–0.38 and $m^* = 0.30$–0.34 for the two spheres used here). As Reynolds number increases from $Re = 300$, the wavelength λ^* decreases slowly, while the amplitudes rise. The phase between the transverse and streamwise vibration (θ_{XY}) appears to

vary continuously with Re, but always remains close to 0°. The amplitudes reach maximum values of $A_Y^* \approx 1.10$ and $A_X^* \approx 0.17$ just prior to $Re = 1550$, after which there is a distinct drop in the amplitude and wavelength. This decrease coincides with the jump in critical mass from 0.4 to 0.6, and with the appearance of the 2R mode, further emphasizing the significance of this transition Reynolds number.

We may also plot contours of amplitude (A^*) and wavelength (λ^*) in the m^*, Re plane, in figure 31. A consistent trend exists for the wavelength: λ^* always decreases as the mass ratio is reduced or as the Reynolds number is increased. In the case of amplitude variation in figure 31, for the lowest Reynolds numbers (Re = 270–500), the nearly vertical orientation of the contours shows that the amplitude is affected mainly by Re. At higher Reynolds numbers ($Re > 3000$), however, the contours are mostly horizontal, indicating a stronger dependence on the mass ratio. Here, the lightest spheres have the largest amplitudes. For spheres that move rectilinearly, the amplitude of any small transient motions can be measured. At all Re, there is a large jump in the amplitude as the critical mass is crossed, clearly separating zigzag motion from the non-vibrating regimes.

In these figures described above, there is clearly a jump in the amplitude (streamwise and transverse to the flow), also a jump in the wavelength as well as the phase angle θ_{XY} across the Reynolds number 1550. It should be noted that this is not simply some artifact of changing the sphere diameter, because even keeping the same diameter, the jump is quite evident as the water–glycerin mix is modified to increase the Reynolds numbers.

Appendix B. Presenting results using the Galileo number Ga

In this study, we have mapped different regimes of motion and wake patterns for rising falling spheres in $\{m^*, Re\}$ space. However, studies of rising and falling bodies sometimes consider the effect of the Galileo number, $Ga = \sqrt{|1 - m^*|\, gD^3}/\nu$, on the body motion, rather than Reynolds number (e.g. Mougin & Magnaudet 2002; Jenny *et al.* 2004; Veldhuis & Biesheuvel 2007). These parameters are easily related. In the case of a sphere that has reached a steady state, the mean drag balances the net buoyancy and weight:

$$F_D = |\pi\rho D^3/6 - m|g. \tag{B 1}$$

Appropriate normalization of (B 1) relates Re and Ga through the drag coefficient according to

$$Re = \sqrt{\frac{4}{3}\frac{1}{C_D}}Ga. \tag{B 2}$$

To predict the dynamics of a particular sphere, parameterizing the problem in terms of $\{m^*, Ga\}$ can be useful. Calculating the Galileo number requires only the properties of the body and of the fluid, and is therefore independent of the motion. Consequently, the sphere may be located immediately in a map of $\{m^*, Ga\}$, such as the one shown in figure 32, for reference. The Reynolds number, on the other hand, is not known *a priori*, since it depends on the terminal velocity, which in turn depends on the sphere dynamics. As a practical matter, however, Re may be approximated by substituting an estimate of the drag coefficient into (B 2). Subsequent iterations may be performed using the drag data provided in figure 12 to obtain a more precise value of Re.

Although the Galileo number allows predictions to be made somewhat more rapidly, the use of the Reynolds number has purpose. The problem being considered

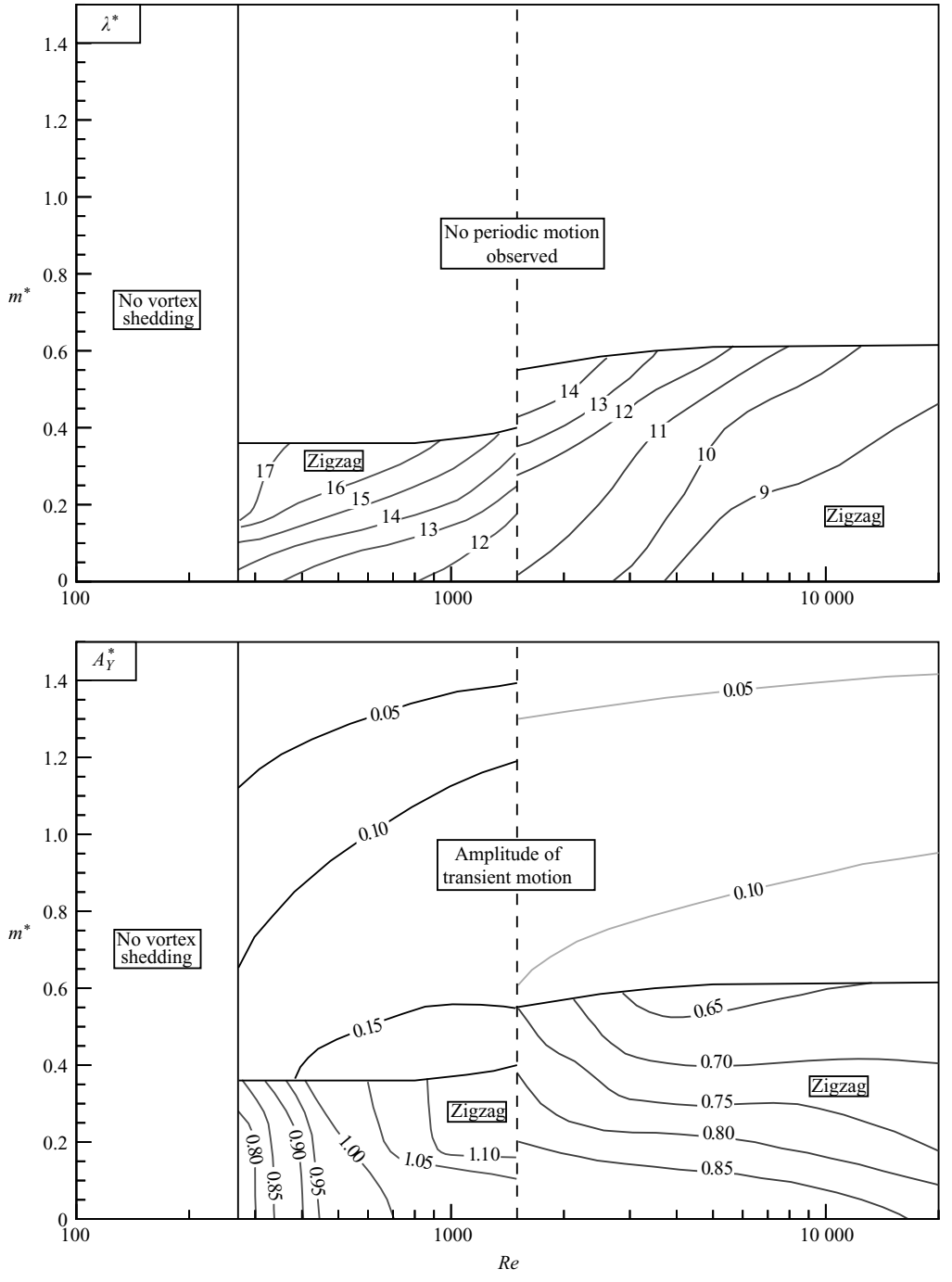

FIGURE 31. Contours of amplitude (A_Y^*) and wavelength (λ^*) in the $\{m^*, Re\}$ plane.

here is of a sphere moving through a fluid under the action of some constant force. The fact that this force happens to be due to gravity is not essential to the dynamics that occur. Moreover, the Galileo number is not defined for flows around bodies that are not moving due to gravity, like fixed or tethered spheres. We have seen

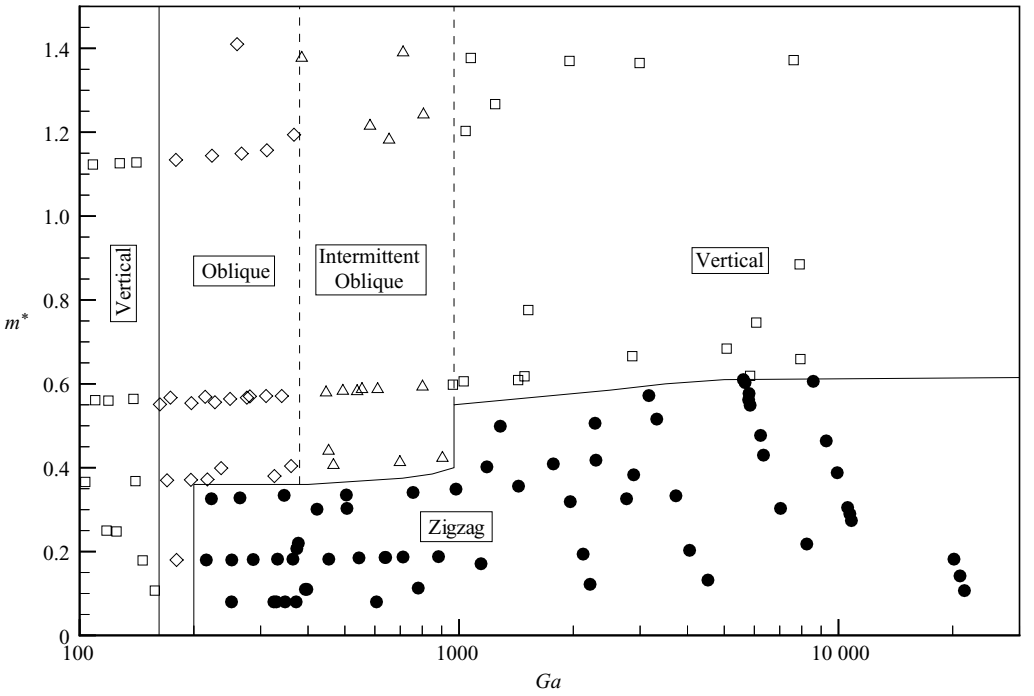

FIGURE 32. Map of regimes of sphere motion in the $\{m^*, Ga\}$ plane.

that comparison with such bodies is useful, for example, in our discussion of wake modes. While the wakes of freely moving spheres have been the subject of relatively few previous studies, they are related to the better-established patterns observed for fixed bodies. Similarly, with knowledge of the Reynolds number, we may compare the present results for the critical mass to experiments using tethered spheres, which yield m^*_{crit} in good agreement with our measurements for freely rising spheres. For each of these systems, there are similarities in the underlying fluid mechanics, and they may be related directly with each other upon employing the Reynolds number.

REFERENCES

ALLEN, H. S. 1900 The motion of a sphere in a viscous fluid: III. *Phil. Mag.* **50**, 519–534.

BACON, D. L. & REID, E. G. 1923 The resistance of spheres in wind tunnels and in air. *Tech. Rep.* No. 185. NACA.

BLOOR, M. S. 1964 The transition to turbulence in the wake of a circular cylinder. *J. Fluid Mech.* **19**, 290–304.

BOILLAT, J. L. & GRAF, W. H. 1981 Settling velocity of spherical particles in calm water. *J. Hydraul. Div. ASCE* **107**, 1123–1131.

BOUCHET, G., MEBAREK, M. & DUŠEK, J. 2006 Hydrodynamic forces acting on a rigid fixed sphere in early transitional regimes. *Eur. J. Mech.* B **25**, 321–336.

BRÜCKER, C. 1999 Structure and dynamics of the wake of bubbles and its relevance for bubble interaction. *Phys. Fluids* **11**, 1781–1796.

BRÜCKER, C. 2001 Spatio-temporal reconstruction of vortex dynamics in axisymmetric wakes. *J. Fluids Struct.* **15**, 543–554.

CHRISTIANSEN, E. B. & BARKER, D. H. 1965 The effect of shape and density on the free settling of particles at high Reynolds numbers. *AIChE J.* **11**, 145–151.

Fabre, D., Auguste, F. & Magnaudet, J. 2008 Bifurcations and symmetry breaking in the wake of axisymmetric bodies. *Phys. Fluids* **20**, 051702.

Fernandes, P. C., Risso, F., Ern, P. & Magnaudet, J. 2007 Oscillatory motion and wake instability of freely rising axisymmetric bodies. *J. Fluid Mech.* **573**, 479–502.

Flemming, F. & Williamson, C. H. K. 2005 Vortex-induced vibrations of a pivoted cylinder. *J. Fluid Mech.* **522**, 215–252.

Goldburg, A. & Florsheim, B. H. 1966 Transition and Strouhal number for the incompressible wake of various bodies. *Phys. Fluids* **9**, 45–50.

Govardhan, R. & Williamson, C. H. K. 2000 Modes of vortex formation and frequency response of a freely vibrating cylinder. *J. Fluid Mech.* **420**, 85–130.

Govardhan, R. & Williamson, C. H. K. 2002 Resonance forever: existence of a critical mass and an infinite regime of resonance in vortex-induced vibration. *J. Fluid Mech.* **473**, 147–166.

Govardhan, R. N. & Williamson, C. H. K. 2005 Vortex-induced vibrations of a sphere. *J. Fluid Mech.* **531**, 11–47.

Gumowski, K., Miedzik, J., Goujon-Durand, S., Jenffer, P. & Wesfried, J. E. 2008 Transition to a time-dependent state of fluid flow in the wake of a sphere. *Phys. Rev.* E **77**, 055308.

Hartman, M. & Yates, J. G. 1993 Free-fall of solid particles through fluids. *Collect. Czech. Chem. Commun.* **58**, 961–982.

Hirsch, P. 1923 Über die Bewegung von Kugeln in ruhenden Flüssigkeiten. *Z. Angew. Math. Mech.* **3**, 93–107.

Horowitz, M. & Williamson, C. H. K. 2006 Dynamics of a rising and falling cylinder. *J. Fluids Struct.* **22**, 837–843.

Horowitz, M. & Williamson, C. H. K. 2008 Critical mass and a new periodic four-ring vortex wake mode for freely rising and falling spheres. *Phys. Fluids* **20**, 101701.

Horowitz, M. & Williamson, C. H. K. Vortex-induced vibration of a rising and falling cylinder. *J. Fluid Mech.* (submitted).

Jauvtis, N. & Williamson, C. H. K. 2004 The effect of two degrees of freedom on vortex-induced vibration at low mass and damping. *J. Fluid Mech.* **509**, 23–62.

Jenny, M., Dušek, J. & Bouchet, G. 2004 Instabilities and transition of a sphere falling or ascending freely in a Newtonian fluid. *J. Fluid Mech.* **508**, 709–720.

Johnson, T. A. & Patel, V. C. 1999 Flow past a sphere up to a Reynolds number of 300. *J. Fluid Mech.* **378**, 19–70.

Karamanev, D. G., Chavarie, C. & Mayer, R. C. 1996 Dynamics of the free rise of a light solid sphere in liquid. *AIChE J.* **42**, 1789–1792.

Kim, D., Choi, H. & Choi, H. 2005 Characteristics of laminar flow past a sphere in uniform shear. *Phys. Fluids* **17**, 103602.

Kim, H. J. & Durbin, P. A. 1988 Observations of the frequencies in a sphere wake and of drag increase by acoustic excitation. *Phys. Fluids* **31**, 3260–3265.

Kuwabara, G., Chiba, S. & Kono, K. 1983 Anomalous motion of a sphere falling through water. *J. Phys. Soc. Japan* **52**, 3373–3381.

Lee, S. 2000 A numerical study of the unsteady wake behind a sphere in a uniform flow at moderate Reynolds numbers. *Comput. Fluids* **29**, 639–667.

Leweke, T., Provansal, M., Ormieres, D. & Lebescond, R. 1999 Vortex dynamics in the wake of a sphere. *Phys. Fluids* **11**, S12.

Liebster, H. 1927 Über den Widerstand von Kugeln. *Ann. Phys.* **82**, 541–562.

Lunnon, R. G. 1926 Fluid resistance to moving spheres. *Proc. R. Soc. Lond.* A **110**, 302–326.

Lunnon, R. G. 1928 Fluid resistance to moving spheres. *Proc. R. Soc. Lond.* A **118**, 680–694.

MacCready, P. B. & Jex, H. R. 1964 Study of sphere motion and balloon wind sensors. *Tech. Rep.* Tech. Mem. X53089. NASA.

Magarvey, R. H. & Bishop, R. L. 1961*a* Transition ranges for three-dimensional wakes. *Can. J. Phys.* **39**, 1418–1422.

Magarvey, R. H. & Bishop, R. L. 1961*b* Wakes in liquid-liquid systems. *Phys. Fluids* **4**, 800–805.

Magnaudet, J. & Eames, I. 2000 The motion of high Reynolds number bubbles in inhomogeneous flows. *Annu. Rev. Fluid Mech.* **32**, 659–708.

Mittal, R. 1999 A Fourier-Chebyshev spectral collocation method for simulating flow past spheres and spheroids. *Intl J. Numer. Methods Fluids* **30**, 921–937.

Mittal, R., Wilson, J. J. & Najjar, F. M. 2002 Symmetry properties of the transitional sphere wake. *AIAA J.* **40**, 579–582.

Möller, W. 1938 Experimentelle Untersuchungen zur Hydrodynamik der Kugel. *Physik. Zeit.* **39**, 58–80.

Mougin, G. & Magnaudet, J. 2002 Wake-induced forces and torques on a zigzagging/spiralling bubble. *Phys. Rev. Lett* **88**, 014502.

Mougin, G. & Magnaudet, J. 2006 Path instability of a rising bubble. *J. Fluid Mech.* **567**, 185–194.

Murrow, H. N. & Henry, R. M. 1965 Self-induced balloon motions. *J. Appl. Meteorol.* **4**, 131–138.

Natarajan, R. & Acrivos, A. 1993 The instability of the steady flow past spheres and disks. *J. Fluid Mech.* **254**, 323–344.

Newton, I. 1726 *Philosophia Naturalis Principia Mathematica,* 3rd edn. Translated by I. B. Cohen and A. Whitman, University of California Press, 1999.

Prasad, A. & Williamson, C. H. K. 1997 The instability of the shear layer separating from a bluff body. *J. Fluid Mech.* **333**, 375–402.

Preukschat, A. W. 1962 Measurements of drag coefficients for falling and rising spheres in free motion. Master's thesis, California Institute of Technology, Pasadena, CA.

Quinn, J. A., Lin, C. H. & Anderson, J. L. 1986 Measuring diffusion coefficients by Taylor's method of hydrodynamic stability. *AIChE J.* **32**, 2028–2033.

Richardson, J. F. & Zaki, W. N. 1954 Sedimentation and fluidisation: part I. *Trans. Inst. Chem. Engrs* **32**, 35–53.

Sakamoto, H. & Haniu, H. 1990 A study on vortex shedding from spheres in a uniform flow. *J. Fluids Engng* **112**, 386–392.

Schlichting, H. 1955 *Boundary Layer Theory*. McGraw-Hill.

Schmidt, F. S. 1920 Zur beschleunigten Bewegung kugelförmiger Körper in widerstehenden Mitteln. *J. Fluid Mech.* **61**, 633–663.

Schmiedel, J. 1928 Experimentelle Untersuchungen über die Fallbewegung von Kugeln und Scheiben in reibenden Flüssigkeiten. *Physik. Zeit.* **17**, 593–610.

Scoggins, J. R. 1964 Aerodynamics of spherical balloon wind sensors. *J. Geophys. Res.* **69**, 591–598.

Shafrir, U. 1965 Horizontal oscillations of falling spheres. *Tech. Rep.* AFCRL 65-141. Air Force Cambridge Research Laboratories.

Shakespear, G. A. 1914 Experiments on the resistance of the air to falling spheres. *Phil. Mag. Ser. 6* **28**, 728–734.

Stringham, G. E., Simons, D. B. & Guy, H. P. 1969 The behaviour of large particles falling in quiescent liquids. US Geological Survey Professional Paper 562C.

Tomboulides, A. G. & Orszag, S. A. 2000 Numerical investigation of transitional and turbulent flow past a sphere. *J. Fluid Mech.* **416**, 45–73.

Veldhuis, C. & Biesheuvel, A. 2007 An experimental study of the regimes of motion of spheres falling or ascending freely in a Newtonian fluid. *Intl J. Multiph. Flow* **33**, 1074–1087.

Veldhuis, C. H. J., Biesheuvel, A. & Lohse, D. 2009 Freely rising light solid spheres. *Intl J. Multiph. Flow* **35**, 312–322.

Veldhuis, C., Biesheuvel, A., van Wijngaarden, L. & Lohse, D. 2005 Motion and wake structure of spherical particles. *Nonlinearity* **18**, C1–C8.

Wieselsberger, C. 1921 Neuere Feststellungen über die Gesetze des Flüssigkeits- und Luftwiderstandes. *Physik. Zeit.* **22**, 321–328.

Williamson, C. H. K. & Govardhan, R. N. 2004 Vortex-induced vibrations. *Annu. Rev. Fluid Mech.* **36**, 413–455.

Williamson, C. H. K. & Roshko, A. 1988 Vortex formation in the wake of an oscillating cylinder. *J. Fluids Struct.* **2**, 355–381.

Wu, M. & Gharib, M. 2002 Experimental studies on the shape and path of small air bubbles rising in clean water. *Phys. Fluids* **14**, L49–L52.